

These results collectively suggest that IGF-1 or IGF1R is sufficient whereas PI3K–Akt pathway is both necessary and sufficient to induce physiological cardiac hypertrophy. A recent study in mice with cardiomyocyte-restricted deletion of IGF1R suggested that cardiac IGF1R signaling could modulate exercise-induced cardiac hypertrophy [20]. In this study, 96 hours of swim training over 5 weeks led to increased AMPK activation in IGF1R-deficient hearts, and AMPK activation was postulated to have a negative impact on cardiac hypertrophy. Insulin receptor (IR)-mediated signals have also been implicated in the regulation of cardiac growth and function. Cardiac-specific IR knockout (CIRKO) mice exhibit small heart size with mildly impaired contractility and reduced Akt activity [21,22], suggesting that IR-mediated signals could potentially play a role in exercise-induced physiological hypertrophy.

To elucidate the role of IGF1R and IR in the development of exercise-induced cardiac hypertrophy, we subjected cardiac-specific IGF1R knockout (CIGFRKO) mice and CIRKO mice to 75 hours of swimming over 4 weeks. Although both CIGFRKO mice and CIRKO mice developed exercise-induced cardiac hypertrophy to the level comparable to their wild type littermates, deletion of a single *Irf* or a single *Igf1r* allele on CIGFRKO or CIRKO background, respectively, blunted hypertrophic responses to exercise. We also observed that tyrosine phosphorylation of both IGF1R and IR was increased in the heart after intravenous IGF-1 administration or exercise training. Thus, IGF-1 and exercise may activate both IGF1R and IR in the heart, and IGF1R- and IR-mediated signals may play redundant roles in the development of cardiac hypertrophy in response to exercise training.

2. Materials and methods

2.1. Animals, exercise training, and IGF-1 administration

CIGFRKO mice were initially generated by crossing *Igf1r*^{flox/flox} mice [23] with α -myosin heavy chain (α MHC)-Cre transgenic mice [24]. Subsequent maintenance of CIGFRKO line was done by crossing CIGFRKO mice (*Igf1r*^{flox/flox}Cre^{+/-}) with *Igf1r*^{flox/flox}Cre^{-/-}

mice. CIRKO mice were generated as described previously [21]. Subsequent maintenance of CIRKO line was done by crossing CIRKO mice (*Irf*^{flox/flox}Cre^{+/-}) with *Irf*^{flox/flox}Cre^{-/-} mice. Cardiac-specific *Igf1r*^{-/-}*Irf*^{+/-} mice and *Igf1r*^{+/-}*Irf*^{-/-} mice were generated by crossing *Igf1r*^{flox/flox}*Irf*^{flox/flox}Cre^{-/-} mice with CIGFRKO mice (*Igf1r*^{flox/flox}*Irf*^{+/+}Cre^{+/-}) and CIRKO mice (*Igf1r*^{+/+}*Irf*^{flox/flox}Cre^{+/-}), respectively. Animals were on a mixed background of C57BL/6J, 129Sv, and FVB, and littermates that contain the same combination of *Igf1r*/*Irf* alleles but do not contain α MHC-Cre transgene were used as wild type controls in each study (Supplementary Fig. S1). Genotyping was performed as described [21,25].

Swimming training was performed in 10-week-old male mice as described previously [26]. Swimming sessions were done twice a day for 28 days. The first 7 days consisted of a training period in which one session was 20 min long on the first day and it was increased by 10 min per day. On the subsequent 21 days, two sessions of 90 min swimming were done. After the final swimming session, mice were overnight fasted and sacrificed. M-mode tracings of left ventricular wall motion at the level of papillary muscle were obtained using Vevo 660 Imaging system (Visual Sonic) with a 25-MHz transducer. For IGF-1 or insulin administration, mice were overnight fasted and anesthetized with pentobarbital, and IGF-1 (Fujisawa Co., Japan) or insulin (Lilly Co., Japan) was intravenously administered. Animals were sacrificed 5 minutes after IGF-1 or insulin administration. All animal procedures were performed with the approval of the Institutional Animal Care and Use Committee of Chiba University.

2.2. Histological analysis

Hearts were fixed and embedded in paraffin for histological analyses. Serial sections of 4 μ m were stained with hematoxylin and eosin (HE) for morphological analysis and Masson's trichrome (MT) for detection of fibrosis. For measurements of myocyte cross-sectional area, immunohistochemistry with anti-dystrophin antibody (Novocastra Laboratories, Newcastle, UK) was performed to visualize myocyte membranes. The sections were reacted with anti-dystrophin

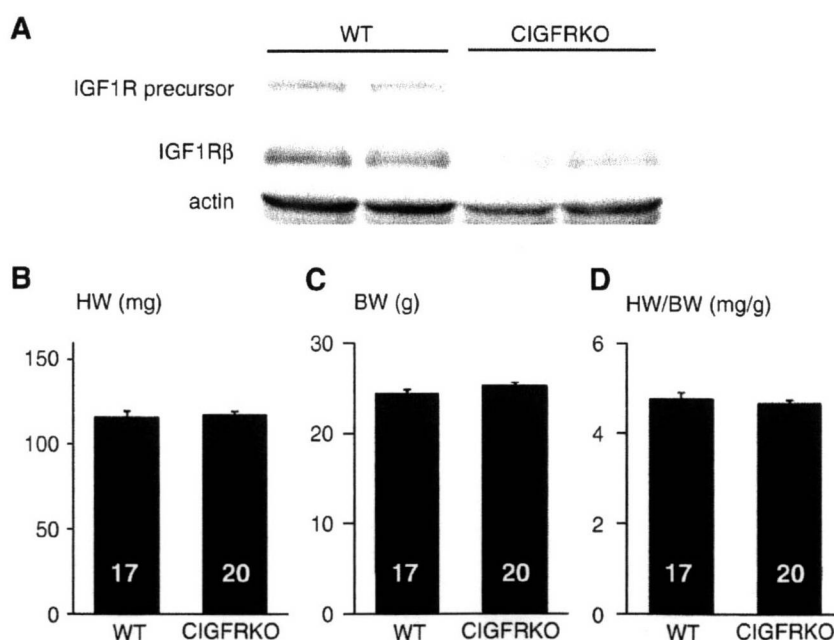


Fig. 1. CIGFRKO mice exhibit no obvious cardiac phenotype at baseline. (A) Expression of IGF1R precursor protein and IGF1R β subunit protein (IGF1R β) as revealed by Western blot analysis of whole heart lysates. Actin served as internal control. (B–D) HW (B), BW (C), and HW/BW ratio (D) of WT and CIGFRKO mice at 10 weeks of age. The number of mice analyzed is shown in the bar.

antibody at 1:20 and visualized by ABC method. Suitable cross-sections for measurements were defined as having round-to-oval membrane staining using ImageJ software. At least 200 myocytes were measured in each sample.

2.3. Western blot analysis and immunoprecipitation

Total protein lysate was extracted from heart tissue and SDS-PAGE was performed as described previously [22]. Anti-IGF1R β , anti-IR β , and anti-phosphotyrosine (PY20) antibodies were from Santa Cruz Biotechnology (Santa Cruz, CA), and anti-actin antibody was from Sigma (St. Louis, MO). For immunoprecipitation, total

heart lysates (500 μ g protein) were precleared with protein G-agarose beads for an hour before incubation with the indicated antibody (1 μ g) overnight at 4 °C. Protein G-agarose beads were added for 3 hours and immunoprecipitates were washed three times in lysis buffer, eluted in 2 \times SDS buffer and subjected to SDS-PAGE.

2.4. Statistical analysis

Data are shown as mean \pm SEM. Statistical significance was determined by Student's t test or Welch's test. P values of <0.05 were considered to be statistically significant.

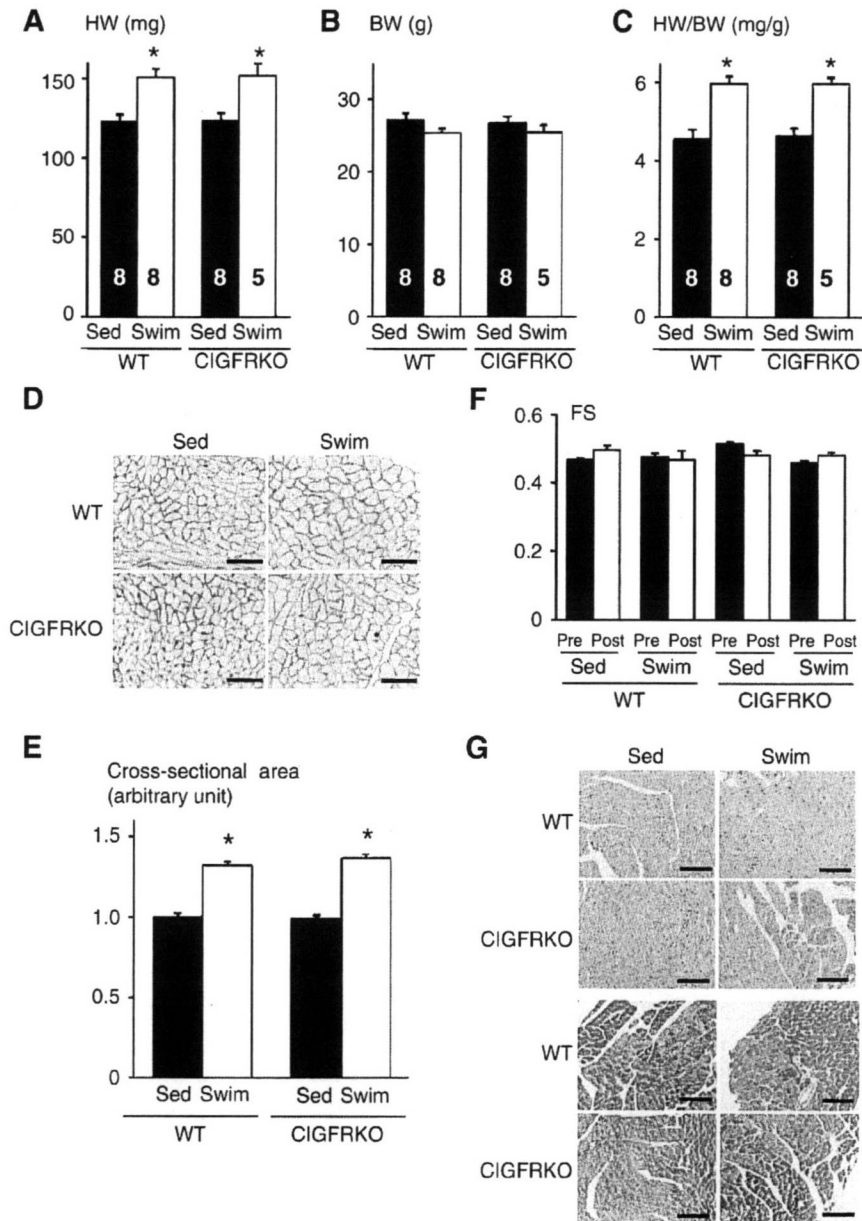


Fig. 2. CIGFRKO mice develop physiological cardiac hypertrophy in response to exercise training. (A–C) HW (A), BW (B), and HW/BW ratio (C) of WT and CIGFRKO mice. * $p < 0.05$ versus Sed group of the same genotype. The number of mice analyzed is shown in the bar. (D) Immunohistochemistry with anti-dystrophin antibody. Scale bar = 50 μ m. (E) Myocyte cross-sectional area of WT and CIGFRKO mice. * $p < 0.05$ versus Sed group of the same genotype. (F) Left ventricular contractile function as assessed by echocardiographic measurement of fractional shortening (FS). Pre and Post represent before and after exercise, respectively. (G) Histological analysis with HE (upper panel) and Masson's trichrome (MT) (lower panel) staining. Scale bar = 100 μ m. Sed and Swim represent a sedentary and a swimming group, respectively.

3. Results

3.1. CIGFRKO mice exhibit no cardiac phenotype at baseline

CIGFRKO mice were initially generated by crossing *Igf1^{flax/flax}* animals with α MHC-Cre transgenic mice, and compared with wild type controls. Western blot analysis of heart lysate revealed that the expression levels of IGF1R precursor protein and IGF1R β subunit protein were reduced, and small amount of proteins detected by western blots were considered to be derived from non-myocytes in the heart (Fig. 1A). At 10 weeks of age, there was no significant difference in heart weight (HW), body weight (BW), heart weight (HW)/BW ratio, and cardiac function as assessed by echocardiography between CIGFRKO mice and wild type (WT) littermates (Figs. 1B–D, and data not shown). Similar results were obtained in other ages. Thus, CIGFRKO mice exhibit no obvious cardiac phenotype at baseline.

3.2. Deletion of *Igf1r* in cardiac myocytes does not attenuate exercise-induced physiological cardiac hypertrophy

Lack of obvious cardiac phenotype in CIGFRKO mice at baseline prompted us to investigate the effect of *Igf1r* deletion on hypertrophic responses of the heart to exercise training. After 75 hours of swimming over 4 weeks, WT and CIGFRKO mice developed similar degrees of cardiac hypertrophy as measured by HW and HW/BW ratio (Figs. 2A–C). The fold increase in myocyte cross-sectional area was also comparable between WT and CIGFRKO animals (Figs. 2D and E). Left ventricular contractile function as measured by echocardiography did not differ between WT and CIGFRKO mice (Fig. 2F), and

histological analyses revealed that there was no interstitial fibrosis or myocyte disarray in the hearts of WT and CIGFRKO mice (Fig. 2G). The presence of Cre recombinase in the heart did not affect the extent of hypertrophy or contractile function following exercise training (Supplementary Fig. S2). These results collectively suggest that exercise-induced physiological cardiac hypertrophy may develop normally in the absence of IGF1R-mediated signals in cardiac myocytes.

3.3. IR is phosphorylated by IGF-1 in the hearts of WT and CIGFRKO mice

Since IGF-1 signaling has been implicated in the development of physiological cardiac hypertrophy, the above-mentioned results were somewhat unexpected. We first examined whether IGF1R-mediated signals were disrupted in cardiac myocytes of CIGFRKO mice. Western blot analysis of whole heart extracts revealed that, although IGF1R protein levels were upregulated after exercise training in the hearts of WT mice, the expression levels of IGF1R remained at low levels both in sedentary and swim-trained CIGFRKO hearts (Fig. 3A). Tyrosine phosphorylation levels of IGF1R and IR were also examined in the heart of WT and CIGFRKO mice after exercise training. Exercise training increased phosphorylation levels of both IGF1R and IR in the heart of WT mice. Increased phosphorylation levels of IGF1R could be in part attributed to upregulation of IGF1R protein levels following exercise training. As expected, IGF1R phosphorylation but not IR phosphorylation was blunted in the heart of CIGFRKO animals (Fig. 3B). IGF1R tyrosine phosphorylation levels were also examined in the hearts of WT and CIGFRKO mice after intravenous IGF-1 administration. Phosphotyrosine blot after IGF1R immunoprecipitation

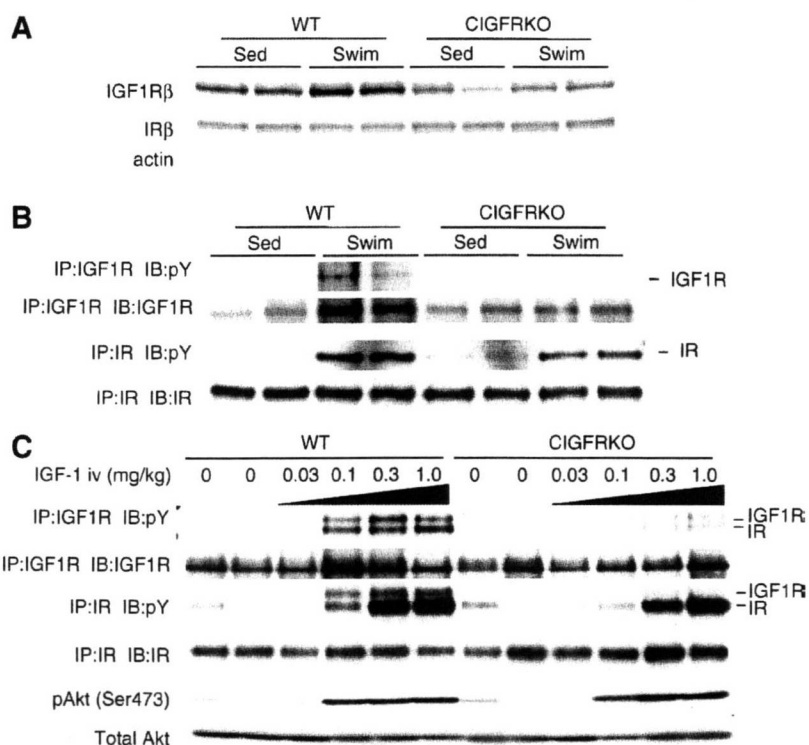


Fig. 3. Western blot analysis of CIGFRKO heart extracts after exercise or IGF-1 administration. (A) Expression of IGF1R β subunit protein (IGF1R β) and IR β subunit protein (IR β) in the heart of WT and CIGFRKO mice. Sed and Swim represent a sedentary and a swimming group, respectively. (B) Tyrosine phosphorylation levels of IGF1R and IR following exercise training. pY represents anti-phosphotyrosine antibody. IP and IB represent immunoprecipitation and immunoblot, respectively. (C) Tyrosine phosphorylation levels of IGF1R/IR and activation of Akt in the heart of WT and CIGFRKO mice 5 minutes after IGF-1 administration. There are some IGF1R bands in the immunoprecipitates of IR and vice versa, possibly due to antibody cross-reactivity. pY represents anti-phosphotyrosine antibody. IP and IB represent immunoprecipitation and immunoblot, respectively.

revealed that tyrosine phosphorylation of IGF1R was markedly reduced in CIGFRKO hearts when compared to that of WT hearts (Fig. 3C, upper panel). These findings strongly suggest that IGF1R-mediated signaling is functionally disrupted in cardiac myocytes of CIGFRKO animals. In the same experimental condition, phosphotyrosine blot after IR immunoprecipitation revealed significant tyrosine phosphorylation of IR both in WT and CIGFRKO hearts after IGF-1 administration (Fig. 3C, middle panel), and phospho-Akt levels in the heart were comparable between WT and CIGFRKO animals (Fig. 3C, lower panel). These observations collectively suggest that IR activated by IGF-1 in part mediates exercise-induced physiological

cardiac hypertrophy and that IR compensates for the loss of IGF1R-mediated signaling in the hearts of CIGFRKO mice following exercise training.

3.4. Deletion of *Ir* in cardiac myocytes does not attenuate exercise-induced physiological cardiac hypertrophy

To test the hypothesis that IR mediates exercise-induced physiological cardiac hypertrophy, CIRKO mice and wild type littermates were subjected to exercise training. After 75 hours of swimming, WT and CIRKO mice exhibited similar degrees of cardiac hypertrophy as

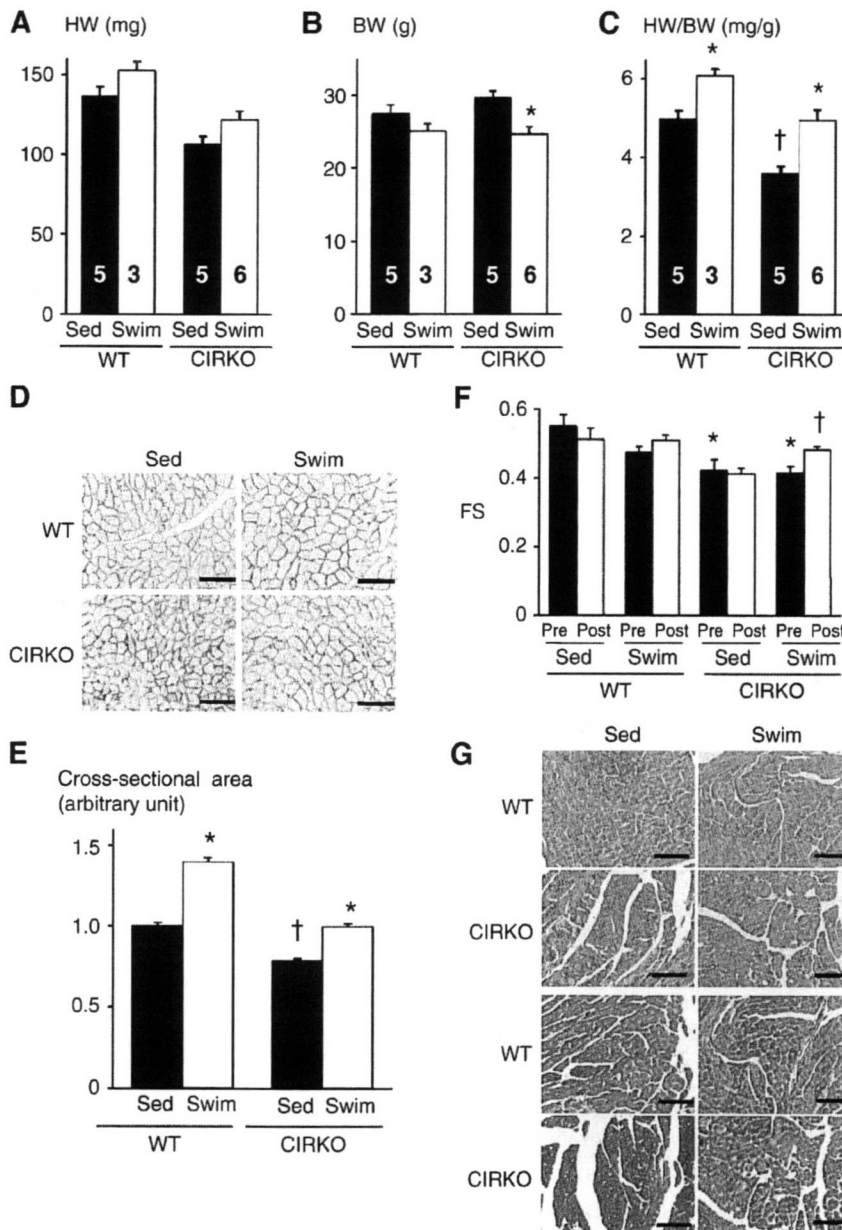


Fig. 4. CIRKO mice develop physiological cardiac hypertrophy in response to exercise training. (A–C) HW (A), BW (B), and HW/BW ratio (C) of WT and CIRKO mice. * $p < 0.05$ versus Sed group of the same genotype, † $p < 0.05$ versus WT Sed group. The number of mice analyzed is shown in the bar. (D) Immunohistochemistry with anti-dystrophin antibody. Scale bar = 50 μm. (E) Myocyte cross-sectional area of WT and CIRKO mice. * $p < 0.05$ versus Sed group of the same genotype, † $p < 0.05$ versus WT Sed group. (F) Left ventricular contractile function as assessed by echocardiographic measurement of fractional shortening (FS). Pre and Post represent before and after exercise, respectively. * $p < 0.05$ versus WT Sed Pre group, † $p < 0.05$ versus CIRKO Swim Pre group. (G) Histological analysis with HE (upper panel) and Masson's trichrome (MT) (lower panel) staining. Scale bar = 100 μm. Sed and Swim represent a sedentary and a swimming group, respectively.

measured by HW (12% versus 14%) and HW/BW ratio (22% versus 38%) (Figs. 4A–C). The fold increase in myocyte cross-sectional area was also significant in WT and CIGFRKO animals (40% and 27%, respectively) (Figs. 4D and E). The relatively enhanced response in HW/BW ratio following exercise was considered to be due to a significant decrease in BW in CIRKO mice following exercise training (Fig. 4B). Interestingly, left ventricular contractile function as assessed by fractional shortening was slightly impaired in CIRKO mice, which was ameliorated by exercise training (Fig. 4F). There was no sign of pathology in histological examination both in WT or CIRKO hearts (Fig. 4G). Thus, exercise-induced physiological cardiac hypertrophy develops normally even in the absence of IR-mediated signals in cardiac myocytes.

Western blot analysis of whole heart extracts revealed that the expression levels of IGF1R were increased in CIRKO hearts at the sedentary state compared to those of WT hearts, and further upregulated after exercise both in WT and CIRKO hearts (Fig. 5A). Tyrosine phosphorylation levels of IGF1R were upregulated both in WT and CIRKO hearts after exercise training, whereas those of IR were upregulated in WT hearts but not in CIRKO hearts (Fig. 5B). When IGF-1 was intravenously administered, phosphotyrosine blot after IGF1R immunoprecipitation revealed that tyrosine phosphorylation of IGF1R was comparable between CIRKO hearts and WT hearts (Fig. 5C, upper panel), whereas phosphotyrosine blot after IR immunoprecipitation revealed that IR tyrosine phosphorylation by IGF-1 was markedly reduced in CIRKO hearts (Fig. 5C, middle panel). Phospho-Akt levels in the heart were comparable between WT and CIRKO animals (Fig. 5C, lower panel). These observations indicate that IR-mediated signals are dispensable for the development of exercise-induced physiological cardiac hypertrophy.

3.5. Combined deletion of *Igf1r* and *Ir* attenuates exercise-induced physiological cardiac hypertrophy

The observation that the deletion of either *Igf1r* alone or *Ir* alone in cardiac myocytes does not attenuate swimming-induced cardiac hypertrophy suggests that IGF1R- and IR-mediated signals could compensate for each other during the development of exercise-induced physiological cardiac growth. To test this hypothesis, we generated compound mutants of *Igf1r* and *Ir* genes in the heart. Homozygous deletion of both genes in cardiac myocytes resulted in severe heart failure and early postnatal lethality (data not shown), consistent with a previous report in which *Igf1r* and *Ir* genes were disrupted in cardiac and skeletal muscle cells [27]. We therefore analyzed mice lacking two *Igf1r* alleles and one *Ir* allele (IGF1R^{-/-}IR^{+/-}) or mice lacking one *Igf1r* allele and two *Ir* alleles (IGF1R^{+/-}IR^{-/-}) in cardiac myocytes.

At sedentary state, HW and HW/BW ratio of IGF1R^{-/-}IR^{+/-} mice was comparable to that of WT mice. When these animals were subjected to 75 hours of swimming, the increase in HW and HW/BW ratio was significantly reduced in IGF1R^{-/-}IR^{+/-} mice compared to WT mice (Figs. 6A–C). The increase in myocyte cross-sectional area was also significantly reduced in IGF1R^{-/-}IR^{+/-} animals compared to WT littermates (Figs. 6D and E). Left ventricular contractile function was not affected by gene deletion and/or exercise training (Fig. 6F), and there was no pathological finding on histology (Fig. 6G). Western blot analysis of whole heart extracts revealed that the expression levels of IR were slightly reduced in IGF1R^{-/-}IR^{+/-} hearts and were not altered by exercise (Fig. 7A). When IGF-1 was intravenously administered, tyrosine phosphorylation of IGF1R was markedly reduced (Fig. 7B, upper panel) and that of IR was also

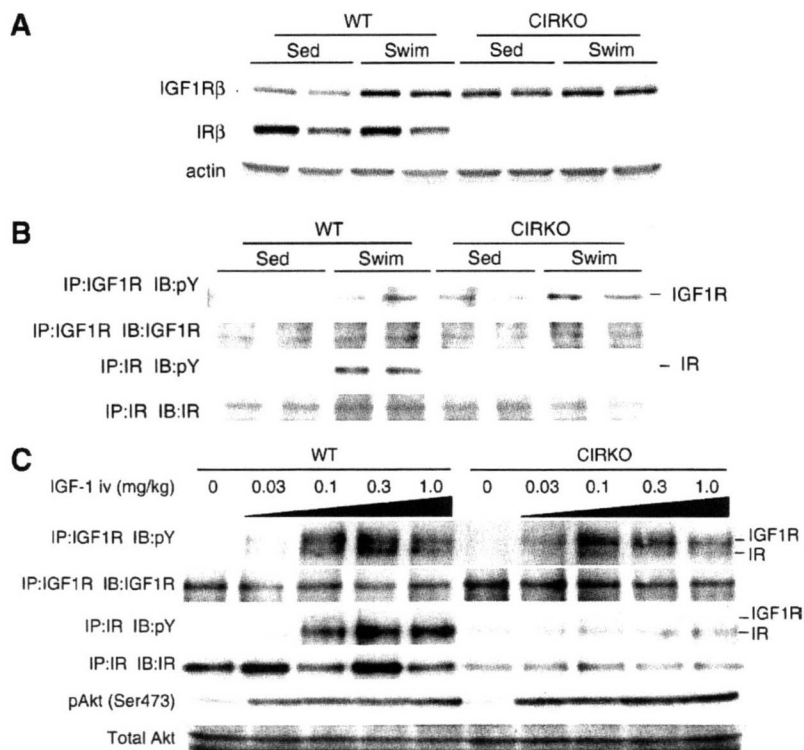


Fig. 5. Western blot analysis of CIRKO heart extracts after exercise or IGF-1 administration. (A) Expression of IGF1R β subunit protein (IGF1Rβ) and IR β subunit protein (IRβ) in the heart of WT and CIRKO mice. Sed and Swim represent a sedentary and a swimming group, respectively. (B) Tyrosine phosphorylation levels of IGF1R and IR following exercise training. pY represents anti-phosphotyrosine antibody. IP and IB represent immunoprecipitation and immunoblot, respectively. (C) Tyrosine phosphorylation levels of IGF1R/IR and activation of Akt in the heart of WT and CIRKO mice 5 minutes after IGF-1 administration. There are some IGF1R bands in the immunoprecipitates of IR and vice versa, possibly due to antibody cross-reactivity. pY represents anti-phosphotyrosine antibody. IP and IB represent immunoprecipitation and immunoblot, respectively.

moderately reduced (Fig. 7B, middle panel). Phospho-Akt levels in the heart were comparable between WT and IGF1R^{-/-}IR^{+/-} animals (Fig. 7B, lower panel).

In contrast to IGF1R^{-/-}IR^{+/-} mice, IGF1R^{+/-}IR^{-/-} mice exhibited small heart size at baseline, and the increase in HW and HW/BW ratio after 4 weeks of swimming was significantly reduced in IGF1R^{+/-}IR^{-/-} mice compared to WT mice (Figs. 8A–C). The increase in myocyte cross-sectional area was also markedly reduced in IGF1R^{+/-}IR^{-/-} animals compared to WT littermates (Figs. 8D and E). Echocardiography revealed a progressive decline in left ventricular contractile function in IGF1R^{+/-}IR^{-/-} mice, which was in part ameliorated by exercise training (Fig. 8F). Histological analysis

demonstrated interstitial fibrosis in the heart of IGF1R^{+/-}IR^{-/-} mice at sedentary state, which was markedly reduced by exercise training (Fig. 8G). Western blot analysis of whole heart extracts revealed that the expression levels of IGF1R were upregulated in IGF1R^{+/-}IR^{-/-} hearts at sedentary state but there was no further upregulation of IGF1R expression after swimming (Fig. 9A). When IGF-1 was intravenously administered, tyrosine phosphorylation of IGF1R was moderately reduced (Fig. 9B, upper panel), and that of IR was markedly reduced (Fig. 9B, middle panel). Phospho-Akt levels in the heart were also reduced in the heart of IGF1R^{+/-}IR^{-/-} animals compared to WT mice (Fig. 9B, lower panel). These observations indicate that IR expressed from a single *Ir* allele is sufficient to

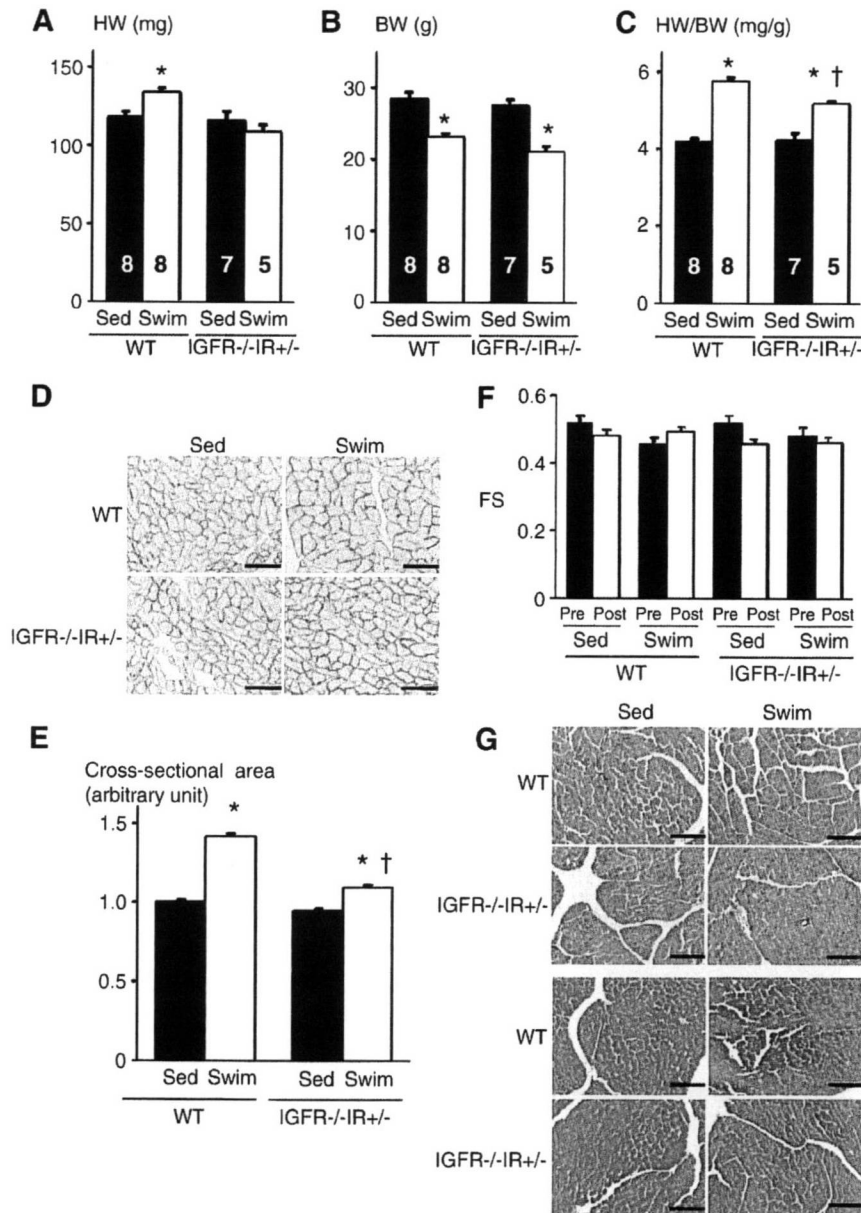


Fig. 6. Exercise-induced physiological cardiac hypertrophy is attenuated in IGF1R^{-/-}IR^{+/-} mice. (A–C) HW (A), BW (B), and HW/BW ratio (C) of WT and IGF1R^{-/-}IR^{+/-} mice. *p<0.05 versus Sed group of the same genotype, †p<0.05 versus WT Swim group. The number of mice analyzed is shown in the bar. (D) Immunohistochemistry with anti-dystrophin antibody. Scale bar = 50 μm. (E) Myocyte cross-sectional area of WT and IGF1R^{-/-}IR^{+/-} mice. *p<0.05 versus Sed group of the same genotype. †p<0.05 versus WT Swim group. (F) Left ventricular contractile function as assessed by echocardiographic measurement of fractional shortening (FS). Pre and Post represent before and after exercise, respectively. (G) Histological analysis with HE (upper panel) and Masson's trichrome (MT) (lower panel) staining. Scale bar = 100 μm. Sed and Swim represent a sedentary and a swimming group, respectively.

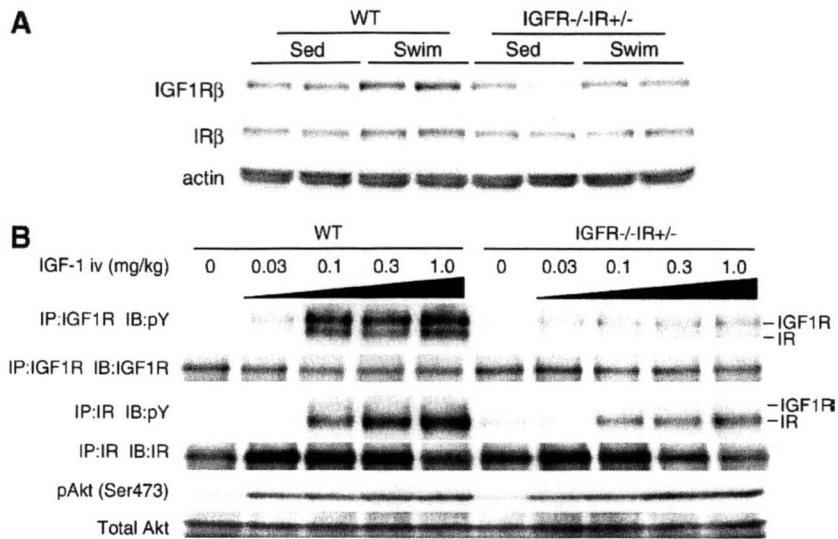


Fig. 7. Western Blot analysis of IGF1R $-/-$ IR $+/-$ heart extracts after exercise or IGF-1 administration. (A) Expression of IGF1R β subunit protein (IGF1R β) and IR β subunit protein (IR β) in the heart of WT and IGF1R $-/-$ IR $+/-$ mice. Sed and Swim represent a sedentary and a swimming group, respectively. (B) Tyrosine phosphorylation levels of IGF1R/IR and activation of Akt in the heart of WT and IGF1R $-/-$ IR $+/-$ mice 5 minutes after IGF-1 administration. There are some IGF1R bands in the immunoprecipitates of IR and vice versa, possibly due to antibody cross-reactivity. pY represents anti-phosphotyrosine antibody. IP and IB represent immunoprecipitation and immunoblot, respectively.

maintain normal postnatal cardiac growth but is insufficient to support the full program of hypertrophic responses to exercise training, whereas IGF1R derived from a single *Igf1r* allele is insufficient both for the maintenance of postnatal cardiac growth/function and for the development of exercise-induced physiological cardiac hypertrophy.

4. Discussion

In the present study, we have dissected the roles of IGF1R and IR in normal postnatal cardiac growth and exercise-induced cardiac hypertrophy. We found that IGF1R and IR have overlapping or redundant functions in these two processes of physiological cardiac growth. We also found that both IGF1R and IR are activated by IGF-1 or exercise, implying that IGF1R- and IR-mediated signals could contribute to hypertrophic responses of the heart to exercise training. These results suggest the existence of a complex signaling network involving IGF1R, IR, and their ligands in the regulation and maintenance of cardiac growth and function (Fig. 10).

Biological actions of insulin and IGF-1 are transduced by IR and IGF1R. These receptors are highly homologous and exist as $\alpha_2\beta_2$ heterodimers, with two extracellular ligand-binding α subunits and two transmembrane β subunits that contain tyrosine kinase domains [28]. There also exists a hybrid IR-IGF1R receptor formed by IR α - β heterodimer and IGF1R α - β heterodimer, which preferentially binds to IGF-1 but not to insulin [29]. Under normal conditions, insulin and IGF-1 signal primarily through their cognate receptors. Thus, insulin signaling acutely regulates glucose metabolism, whereas IGF-1 signaling regulates embryonic and postnatal body/organ size. This notion is supported by distinct phenotypes of IR and IGF1R knockout mice: IR-deficient mice are perinatally lethal due to severe ketoacidosis, whereas IGF1R-deficient mice exhibit severe growth retardation (~45% of normal size) [30]. However, it is probably an oversimplification to view that IR mediates metabolic actions and IGF1R mediates growth. Indeed, IR-deficient mice are slightly smaller than wild type mice (~90% of normal size), and combined deletion of IR and IGF1R results in more severe growth retardation (~30% of normal size) than IGF1R single deletion [30]. Thus, IR and IGF1R have functional redundancies in mediating growth promoting effects during embryonic development.

We previously reported that CIRKO mice exhibit a small heart phenotype (~80% of the wild type heart size). Based on the observation that IGF1R-deficient mice show more severe growth retardation than IR-deficient mice [30], we initially hypothesized that IGF1R-mediated signals would play a dominant role over IR-mediated signals in normal postnatal cardiac growth. However, we found that there was no obvious cardiac phenotype in CIRKO mice at baseline. Furthermore, simultaneous deletion of *Ir* and *Igf1r* in cardiac myocytes resulted in perinatal lethality with contractile dysfunction and reduced heart size (data not shown). These observations suggest that IR and IGF1R have functional redundancies in mediating postnatal cardiac growth and that IR plays a dominant role over IGF1R in this process. Although the basis for differential contribution of IR and IGF1R to embryonic development (IR<IGF1R) versus postnatal heart growth (IR>IGF1R) is not clear, it may be due to differences in relative expression levels of IR, IGF1R, and their ligands during embryonic versus postnatal development.

The lack of obvious cardiac phenotype in CIRKO mice prompted us to investigate the effect of *Igf1r* deletion in the heart under stressed conditions. Previous studies implicated a critical role of IGF-1-PI3K-Akt pathway in the development of exercise-induced physiological cardiac hypertrophy [9,10]. Specifically, gain-of-function studies in transgenic mice revealed that IGF1R is capable of inducing physiological cardiac growth [14]. We therefore hypothesized that hypertrophic responses to exercise training might be impaired in the heart of CIRKO mice. Unexpectedly, however, both wild type and CIRKO mice developed comparable levels of cardiac hypertrophy in response to swimming training. In addition, IGF-1 administration or exercise training induced extensive tyrosine phosphorylation of IR in the heart of wild type and CIRKO mice. On the contrary, insulin administration induced robust phosphorylation of IR but not IGF1R (Supplementary Fig. S3). These findings suggest that both IGF1R and IR can be activated by IGF-1 and may contribute to the development of exercise-induced cardiac hypertrophy in a functionally redundant fashion. This notion was further supported by our studies in CIRKO, IGF1R $-/-$ IR $+/-$, and IGF1R $+/-$ IR $-/-$ mice, in which combined deletion of *Igf1r* and *Ir* gene in cardiac myocytes attenuated hypertrophic responses of the heart to exercise training whereas deletion of *Ir* gene alone did not. Furthermore, the observation that IGF1R $+/-$ IR $-/-$ mice were more severely impaired in hypertrophic

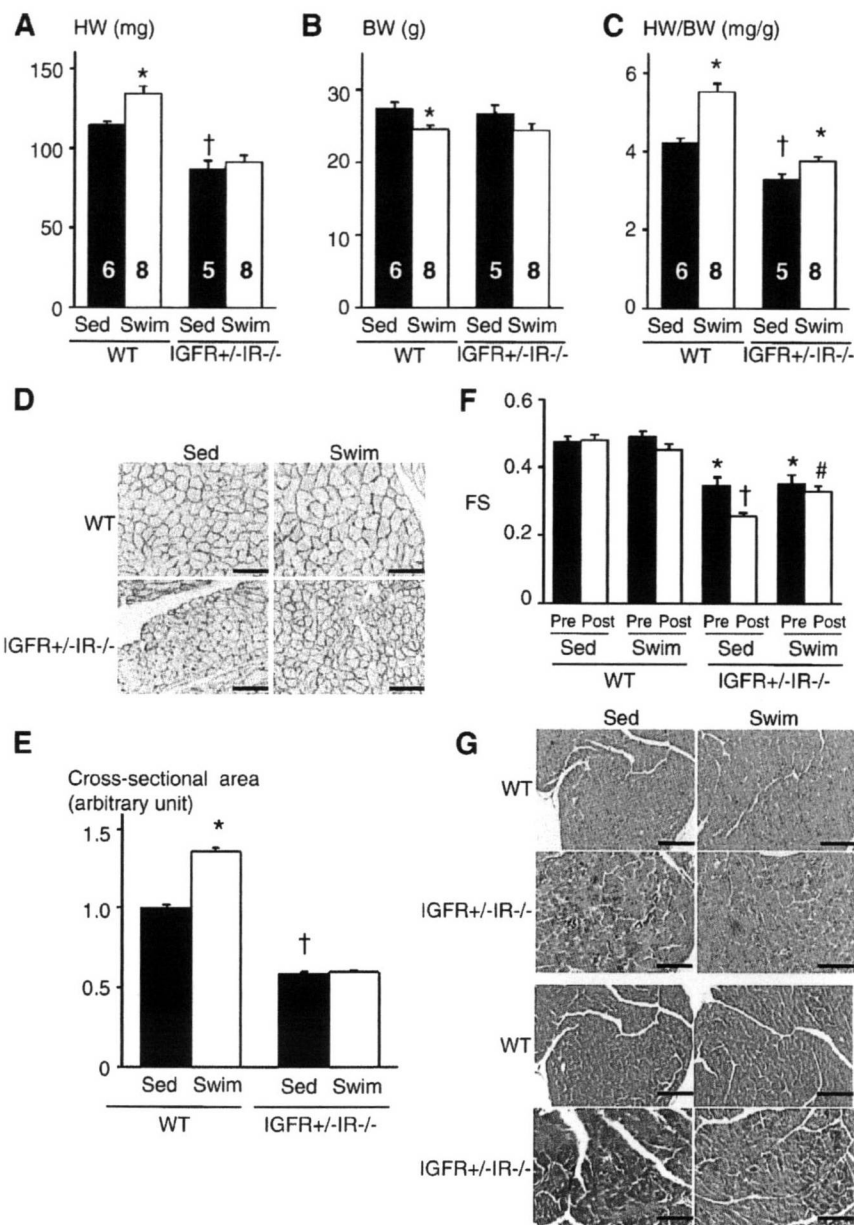


Fig. 8. Exercise-induced physiological cardiac hypertrophy is attenuated in IGF1R+/-IR-/- mice. (A–C) HW (A), BW (B), and HW/BW ratio (C) of WT and IGF1R+/-IR-/- mice. **p* < 0.05 versus Sed group of the same genotype, †*p* < 0.05 versus WT Sed group. The number of mice analyzed is shown in the bar. (D) Immunohistochemistry with anti-dystrophin antibody. Scale bar = 50 μm. (E) Myocyte cross-sectional area of WT and IGF1R+/-IR-/- mice. **p* < 0.05 versus WT Sed group, †*p* < 0.05 versus WT Sed group. (F) Left ventricular contractile function as assessed by echocardiographic measurement of fractional shortening (FS). Pre and Post represent before and after exercise, respectively. **p* < 0.05 versus WT Sed Pre group, †*p* < 0.05 versus IGF1R+/-IR-/- Sed Pre group, #*p* < 0.05 versus IGF1R+/-IR-/- Sed Post group. (G) Histological analysis with HE (upper panel) and Masson's trichrome (MT) (lower panel) staining. Scale bar = 100 μm. Sed and Swim represent a sedentary and a swimming group, respectively.

responses to exercise than IGF1R-/-IR+/- mice suggests that IR-mediated signals might play a dominant role over those mediated by IGF1R in exercise-induced cardiac hypertrophy, as is the case with normal postnatal cardiac growth. Our results also suggest the possibility that the small heart phenotype of CIRKO mice is in part due to the impairment of IR signals activated by IGF-1 or IGF-2 but not by insulin.

The IGF-1–PI3K–Akt pathway has been implicated in physiological cardiac growth. However, the precise mechanism by which this signaling pathway regulates cardiac growth is not completely understood. Although IR appears to be activated by IGF-1 in the heart, the binding affinity of IGF-1 to IR has been reported to be ~100-fold lower relative to that of insulin to IR. One possible mechanism of

cross talk between IGF-1 and IR is the ability of IGF1R-IR hybrid receptors to bind to IGF-1 but not to insulin. It was also recently shown that IGF-1 activates IR at physiological concentrations in murine fibroblasts [31]. In this case, IGF-1 selectively activates IRS-2 and the PI3K pathway but not the IRS-1 and ERK pathway. These and other potential mechanisms of IR activation by IGF-1 could contribute to the development of exercise-induced cardiac hypertrophy.

Kim et al. [20] recently reported that exercise-induced cardiac hypertrophy is attenuated in CIGFRKO mice and that activation of AMPK in the heart of CIGFRKO mice is a potential mechanism leading to impaired hypertrophic responses in these animals. However, we could not detect significant differences in cardiac AMPK activity between WT and CIGFRKO mice either before or after exercise. An

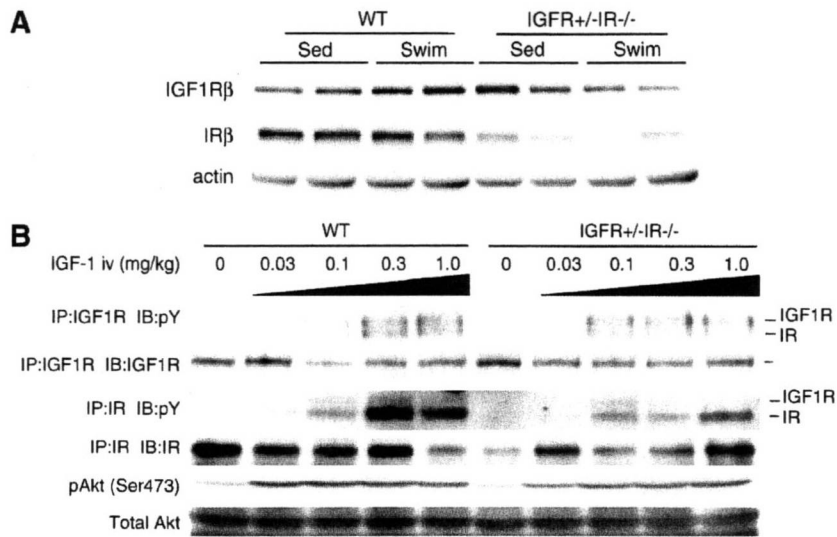


Fig. 9. Western blot analysis of IGF1R^{+/−}IR^{−/−} heart extracts after exercise or IGF-1 administration. (A) Expression of IGF1Rβ subunit protein (IGF1Rβ) and IRβ subunit protein (IRβ) in the heart of WT and IGF1R^{+/−}IR^{−/−} mice. Sed and Swim represent a sedentary and a swimming group, respectively. (B) Tyrosine phosphorylation levels of IGF1R/IR and activation of Akt in the heart of WT and IGF1R^{+/−}IR^{−/−} mice 5 minutes after IGF-1 administration. There are some IGF1R bands in the immunoprecipitates of IR and vice versa, possibly due to antibody cross-reactivity. pY represents anti-phosphotyrosine antibody. IP and IB represent immunoprecipitation and immunoblot, respectively.

important difference between Kim's study and our own is that the study of Kim et al used a more protracted exercise protocol (96 hours total over 5 weeks) at a higher altitude (4000 ft above sea level). This might be the reason for the activation of AMPK in CIGFRKO mice in those studies but not in ours. In addition, Kim et al. [20] reported that Akt activity was not altered between CIGFRKO mice and wild type mice after exercise training, although the degree of exercise-induced cardiac hypertrophy was significantly reduced in CIGFRKO animals. In the present study, although exercise-induced cardiac hypertrophy was impaired in IGF1R^{−/−}IR^{+/−} mice, phospho-Akt levels of IGF1R^{−/−}IR^{+/−} mice were comparable to those of wild type mice (Fig. 7B). Likewise, although exercise-induced cardiac hypertrophy was severely impaired in IGF1R^{+/−}IR^{−/−} mice, phospho-Akt levels in the heart were only slightly impaired in IGF1R^{+/−}IR^{−/−} mice compared to those in wild type mice (Fig. 9B). Thus, the level of activation of Akt does not necessarily correlate with the degree of cardiac hypertrophy in *Igf1r* and *Igf1r/Ir* compound mutant mice. Taken together, these two studies would suggest that deficiency of IGF-1 signaling in the heart does not prevent exercise-induced cardiac hypertrophy on the basis of reduced signaling via the IGF1R to Akt, but may impact cardiac hypertrophy by indirect mechanisms. Our data would suggest that these mechanisms become amplified when insulin and IGF-1 signaling are simultaneously impaired.

In summary, we have demonstrated overlapping roles of IGF1R- and IR-mediated signals in the development of exercise-induced physiological cardiac hypertrophy (Fig. 10). The cross talk between IGF1R- and IR-mediated signals might be in part at the level of ligand-receptor interaction at the cell surface. Further elucidation of the signaling pathways downstream of the insulin and IGF-1 receptors that modulate physiological cardiac hypertrophy might identify novel targets that could be exploited in the management of heart failure, where evidence exists that function and prognosis might be increased by exercise.

Acknowledgments

We thank E. Fujita, R. Kobayashi, and Y. Ishiyama for technical assistance. This work was supported by grants from the Ministry of Education, Culture, Sports, Science and Technology (MEXT) to I.K. and by NIH grant RO1HL070070 to E.D.A.

Appendix A. Supplementary data

Supplementary data associated with this article can be found, in the online version, at doi:10.1016/j.yjmcc.2009.08.028.

References

- [1] Pasumarthi KB, Field LJ. Cardiomyocyte cell cycle regulation. *Circ Res* 2002;90:1044–54.
- [2] Olson EN, Schneider MD. Sizing up the heart: development redux in disease. *Genes Dev* 2003;17:1937–56.
- [3] Richey PA, Brown SP. Pathological versus physiological left ventricular hypertrophy: a review. *J Sports Sci* 1998;16:129–41.
- [4] Heineke J, Molkenin JD. Regulation of cardiac hypertrophy by intracellular signalling pathways. *Nat Rev Mol Cell Biol* 2006;7:589–600.
- [5] Coats AJ. Exercise training for heart failure: coming of age. *Circulation* 1999;99:1138–40.
- [6] Konhilas JP, Watson PA, Maass A, Boucek DM, Horn T, Stauffer BL, Luckey SW, Rosenberg P, Leinwand LA. Exercise can prevent and reverse the severity of hypertrophic cardiomyopathy. *Circ Res* 2006;98:540–8.
- [7] McMullen JR, Amirahmadi F, Woodcock EA, Schinke-Braun M, Bouwman RD, Hewitt KA, Mollica JP, Zhang L, Zhang Y, Shioi T, Buerger A, Izumo S, Jay PY, Jennings GL. Protective effects of exercise and phosphoinositide 3-kinase (p110α) signaling in dilated and hypertrophic cardiomyopathy. *Proc Natl Acad Sci U S A* 2007;104:612–7.
- [8] Scheuer J, Malhotra A, Hirsch C, Capasso J, Schaible TF. Physiologic cardiac hypertrophy corrects contractile protein abnormalities associated with pathologic hypertrophy in rats. *J Clin Invest* 1982;70:1300–5.
- [9] Shiojima I, Walsh K. Regulation of cardiac growth and coronary angiogenesis by the Akt/PKB signaling pathway. *Genes Dev* 2006;20:3347–65.
- [10] Dorn Jr GW. The fuzzy logic of physiological cardiac hypertrophy. *Hypertension* 2007;49:962–70.
- [11] Neri Serneri GG, Boddì M, Modesti PA, Cecioni I, Coppo M, Padeletti L, Michelucci A, Colella A, Galanti G. Increased cardiac sympathetic activity and insulin-like growth factor-I formation are associated with physiological hypertrophy in athletes. *Circ Res* 2001;89:977–82.
- [12] Scheinowitz M, Kessler-Ickelson G, Freimann S, Zimmermann R, Schaper W, Golomb E, Savion N, Eldar M. Short- and long-term swimming exercise training increases myocardial insulin-like growth factor-1 gene expression. *Growth Horm IGF Res* 2003;13:19–25.
- [13] Delaughter MC, Taffet GE, Fiorotto ML, Entman ML, Schwartz RJ. Local insulin-like growth factor I expression induces physiologic, then pathologic, cardiac hypertrophy in transgenic mice. *FASEB J* 1999;13:1923–9.
- [14] McMullen JR, Shioi T, Huang WY, Zhang L, Tarnavski O, Bisping E, Schinke M, Kong S, Sherwood MC, Brown J, Riggi L, Kang PM, Izumo S. The insulin-like growth factor 1 receptor induces physiological heart growth via the phosphoinositide 3-kinase (p110α) pathway. *J Biol Chem* 2004;279:4782–93.
- [15] Shioi T, Kang PM, Douglas PS, Hampe J, Yballe CM, Lawitts J, Cantley LC, Izumo S. The conserved phosphoinositide 3-kinase pathway determines heart size in mice. *EMBO J* 2000;19:2537–48.

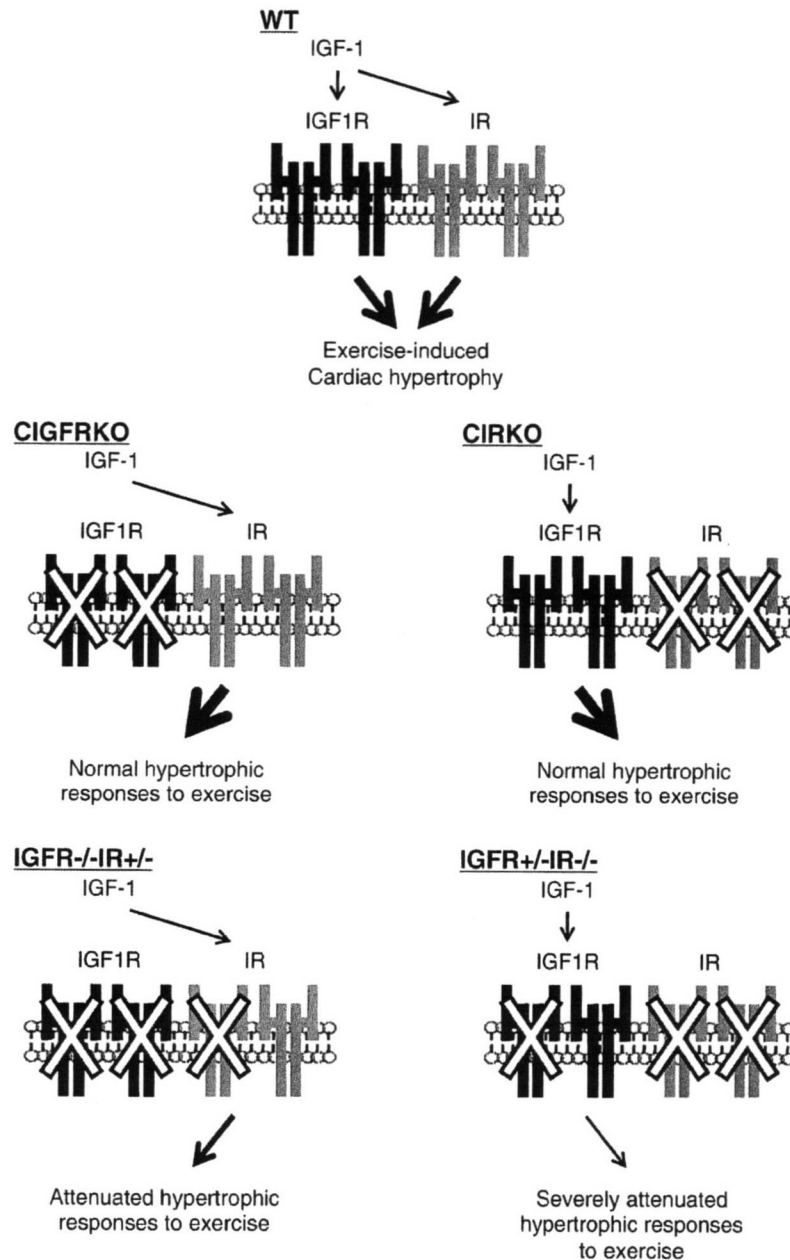


Fig. 10. Schematic illustration of the interaction and cross talk between IGF1R- and IR-mediated signals in exercise-induced cardiac hypertrophy. IGF-1 activates both IGF1R and IR in the heart in response to exercise training. Exercise-induced cardiac hypertrophy develops normally in CIGFRKO mice and CIRKO mice, although combined deletion of two *Igf1r* alleles and one *Ir* allele or one *Igf1r* allele and two *Ir* alleles results in the attenuation of exercise-induced hypertrophy. Thus, exercise-induced cardiac hypertrophy is mediated both by IGF1R- and IR-mediated signals in a redundant fashion. IGF-1 appears to be a major factor that activates both IGF1R and IR. The contribution of insulin in exercise-induced cardiac hypertrophy is not clear from our present study.

- [16] McMullen JR, Shioi T, Zhang L, Tarnavski O, Sherwood MC, Kang PM, Izumo S. Phosphoinositide 3-kinase(p110alpha) plays a critical role for the induction of physiological, but not pathological, cardiac hypertrophy. *Proc Natl Acad Sci U S A* 2003;100:12355–60.
- [17] Condorelli G, Drusco A, Stassi G, Bellacosa A, Roncarati R, Iaccarino G, Russo MA, Gu Y, Dalton N, Chung C, Latronico MV, Napoli C, Sadoshima J, Croce CM, Ross Jr J. Akt induces enhanced myocardial contractility and cell size in vivo in transgenic mice. *Proc Natl Acad Sci U S A* 2002;99:12333–8.
- [18] Shiojima I, Sato K, Izumiya Y, Schiekhofer S, Ito M, Liao R, Colucci WS, Walsh K. Disruption of coordinated cardiac hypertrophy and angiogenesis contributes to the transition to heart failure. *J Clin Invest* 2005;115:2108–18.
- [19] DeBosch B, Treskov I, Lupu TS, Weinheimer C, Kovacs A, Courtois M, Muslin AJ. Akt1 is required for physiological cardiac growth. *Circulation* 2006;113:2097–104.
- [20] Kim J, Wende AR, Sena S, Theobald HA, Soto J, Sloan C, Wayment BE, Litwin SE, Holzenberger M, Leroith D, Abel ED. IGF-1 receptor signaling is required for exercise-induced cardiac hypertrophy. *Mol Endocrinol* 2008;22:2531–43.
- [21] Belke DD, Betuing S, Tuttle MJ, Gravelleau C, Young ME, Pham M, Zhang D, Cooksey RC, McClain DA, Litwin SE, Taegtmeier H, Severson D, Kahn CR, Abel ED. Insulin signaling coordinately regulates cardiac size, metabolism, and contractile protein isoform expression. *J Clin Invest* 2002;109:629–39.
- [22] Shiojima I, Yefremashvili M, Luo Z, Kureishi Y, Takahashi A, Tao J, Rosenzweig A, Kahn CR, Abel ED, Walsh K. Akt signaling mediates postnatal heart growth in response to insulin and nutritional status. *J Biol Chem* 2002;277:37670–7.
- [23] Holzenberger M, Leneuve P, Hamard G, Ducos B, Perin L, Binoux M, Le Bouc Y. A targeted partial invalidation of the insulin-like growth factor I receptor gene in mice causes a postnatal growth deficit. *Endocrinology* 2000;141:2557–66.
- [24] Abel ED, Kaulbach HC, Tian R, Hopkins JC, Duffy J, Doetschman T, Minnemann T, Boers ME, Hadro E, Oberste-Berghaus C, Quist W, Lowell BB, Ingwall JS, Kahn BB. Cardiac hypertrophy with preserved contractile function after selective deletion of GLUT4 from the heart. *J Clin Invest* 1999;104:1703–14.
- [25] Leneuve P, Zaoui R, Monget P, Le Bouc Y, Holzenberger M. Genotyping of Cre-lox mice and detection of tissue-specific recombination by multiplex PCR. *Biotechniques* 2001;31:1156–60,1162.

- [26] Oka T, Maillet M, Watt AJ, Schwartz RJ, Aronow BJ, Duncan SA, Molkentin JD. Cardiac-specific deletion of Gata4 reveals its requirement for hypertrophy, compensation, and myocyte viability. *Circ Res* 2006;98:837–45.
- [27] Laustsen PG, Russell SJ, Cui L, Entingh-Pearsall A, Holzenberger M, Liao R, Kahn CR. Essential role of insulin and insulin-like growth factor 1 receptor signaling in cardiac development and function. *Mol Cell Biol* 2007;27:1649–64.
- [28] Taniguchi CM, Emanuelli B, Kahn CR. Critical nodes in signalling pathways: insights into insulin action. *Nat Rev Mol Cell Biol* 2006;7:85–96.
- [29] Slaaby R, Schaffer L, Lautrup-Larsen I, Andersen AS, Shaw AC, Mathiasen IS, Brandt J. Hybrid receptors formed by insulin receptor (IR) and insulin-like growth factor I receptor (IGF-IR) have low insulin and high IGF-1 affinity irrespective of the IR splice variant. *J Biol Chem* 2006;281:25869–74.
- [30] Rother KI, Accili D. Role of insulin receptors and IGF receptors in growth and development. *Pediatr Nephrol* 2000;14:558–61.
- [31] Denley A, Carroll JM, Brierley GV, Cosgrove L, Wallace J, Forbes B, Roberts Jr CT. Differential activation of insulin receptor substrates 1 and 2 by insulin-like growth factor-activated insulin receptors. *Mol Cell Biol* 2007;27:3569–77.



Cardiac mast cells cause atrial fibrillation through PDGF-A–mediated fibrosis in pressure-overloaded mouse hearts

Chien-hui Liao,^{1,2} Hiroshi Akazawa,¹ Masaji Tamagawa,³ Kaoru Ito,¹ Noritaka Yasuda,¹ Yoko Kudo,¹ Rie Yamamoto,¹ Yukako Ozasa,¹ Masanori Fujimoto,¹ Ping Wang,¹ Hiromitsu Nakauchi,² Haruaki Nakaya,³ and Issei Komuro¹

¹Department of Cardiovascular Science and Medicine, Chiba University Graduate School of Medicine, Chiba, Japan.

²Division of Stem Cell Therapy, Center for Stem Cell and Regenerative Medicine, Institute of Medical Science, University of Tokyo, Tokyo, Japan. ³Department of Pharmacology, Chiba University Graduate School of Medicine, Chiba, Japan.

Atrial fibrillation (AF) is a common arrhythmia that increases the risk of stroke and heart failure. Here, we have shown that mast cells, key mediators of allergic and immune responses, are critically involved in AF pathogenesis in stressed mouse hearts. Pressure overload induced mast cell infiltration and fibrosis in the atrium and enhanced AF susceptibility following atrial burst stimulation. Both atrial fibrosis and AF inducibility were attenuated by stabilization of mast cells with cromolyn and by BM reconstitution from mast cell-deficient WBB6F1-Kit^{W/W^v} mice. When cocultured with cardiac myocytes or fibroblasts, BM-derived mouse mast cells increased platelet-derived growth factor A (PDGF-A) synthesis and promoted cell proliferation and collagen expression in cardiac fibroblasts. These changes were abolished by treatment with a neutralizing antibody specific for PDGF α -receptor (PDGFR- α). Consistent with these data, upregulation of atrial *Pdgfra* expression in pressure-overloaded hearts was suppressed by BM reconstitution from WBB6F1-Kit^{W/W^v} mice. Furthermore, injection of the neutralizing PDGFR- α -specific antibody attenuated atrial fibrosis and AF inducibility in pressure-overloaded hearts, whereas administration of homodimer of PDGF-A (PDGF-AA) promoted atrial fibrosis and enhanced AF susceptibility in normal hearts. Our results suggest a crucial role for mast cells in AF and highlight a potential application of controlling the mast cell/PDGF-A axis to achieve upstream prevention of AF in stressed hearts.

Introduction

Atrial fibrillation (AF) is a supraventricular arrhythmia that is characterized by rapid and fibrillatory atrial activation with an irregular ventricular response. AF remains the most common arrhythmia encountered in clinical practice and is associated with an increased risk of stroke, heart failure, and overall mortality (1). Several cardiovascular disorders predispose to AF, such as coronary artery disease, valvular heart disease, congestive heart failure, and hypertension, especially when LV hypertrophy is present (1). Recent electrophysiological evidence has indicated that the triggering ectopic foci act on predisposing substrates to initiate single- or multiple-circuit reentry, leading to AF (2). The most important histopathological change in AF is atrial fibrosis (3, 4). Accumulation of ECM proteins has been documented in biopsied specimens of atrium from patients with AF (5), and experimental studies using animal models have indicated that interstitial deposition of dense ECM proteins causes separation between bundles of atrial myocytes and disturbs cell-to-cell impulse propagation (3, 4). In addition, atrial fibrosis potentially exaggerates myocardial ischemia by hampering oxygen diffusion and alters the electrophysical and biomechanical properties of atrial myocytes, allowing the initiation and perpetuation of AF (4). The mechanisms underlying the development of atrial fibrosis in AF remain unclear, but evolving evidence has suggested that inflammation is profoundly implicated in the process of

the structural remodeling in the atrium (4, 6). Inflammatory infiltrates were observed in the atrium of AF patients and animal models (7, 8). Furthermore, inflammatory biomarkers such as C-reactive protein were elevated in AF patients and were associated with the presence of AF and the future development of AF (9, 10). However, it remains to be fully elucidated how inflammation is linked to the development of structural remodeling as a susceptible AF substrate in stressed hearts.

Mast cells function as key effector cells during allergic and immune responses through releasing preformed or newly synthesized bioactive products (11). Recent studies have implicated mast cells in inflammation and tissue remodeling (11, 12). Indeed, mast cells reside in many tissues including the heart (13) and participate in the inflammatory process underlying several cardiovascular disorders, such as atherosclerosis (14, 15), aortic aneurysm (16, 17), heart failure (18), viral myocarditis (19), and ventricular arrhythmia during ischemia/reperfusion injury (20). In particular, mast cell-derived IL-6 and IFN- γ have been reported to promote atherosclerosis and abdominal aortic aneurysm (15, 16). Meanwhile, mast cells enhance the fibrogenic process through the release of multiple proteases and inflammatory cytokines in the skin, lung, and kidney (21–24). Here, we demonstrate that mast cells infiltrate the atrium of pressure-overloaded mice and contribute to the pathogenesis of atrial fibrosis and AF susceptibility. Mechanistically, upregulation of PDGF-A mediates the fibrogenic effect of mast cells in promoting AF. These results provide mechanistic insights into the pathogenic role of mast cells in promoting an AF substrate in stressed hearts.

Conflict of interest: The authors have declared that no conflict of interest exists.

Citation for this article: *J. Clin. Invest.* 120:242–253 (2010). doi:10.1172/JCI39942.



Table 1
Echocardiographic measurements in TAC- and sham-operated mice with or without treatment with cromolyn

Cromolyn	Sham		TAC	
	(-)	(+)	(-)	(+)
Number	10	5	17	15
HW/BW (mg/g)	4.55 ± 0.11	4.64 ± 0.04	5.24 ± 0.05 ^A	5.54 ± 0.13 ^A
HR (bpm)	610.10 ± 7.59	613.20 ± 3.44	599.24 ± 7.30	622.67 ± 7.05
LVDd (mm)	3.58 ± 0.08	3.51 ± 0.08	3.55 ± 0.04	3.54 ± 0.09
LVDs (mm)	1.99 ± 0.06	2.06 ± 0.05	2.05 ± 0.04	1.97 ± 0.07
FS (%)	44.5 ± 0.87	41.2 ± 0.99	42.2 ± 0.62	44.6 ± 0.91
LVPWth (mm)	0.65 ± 0.11	0.64 ± 0.04	0.81 ± 0.01 ^A	0.82 ± 0.01 ^A

^A*P* < 0.01 versus sham. FS, fractional shortening; HR, heart rate; HW/BW, heart-to-body weight ratio; LVDd, LV diameter in end diastole; LVDs, LV diameter in end systole; LVPWth, LV posterior wall thickness in end diastole.

Results

Atrial burst stimulation induces AF in pressure-overloaded hearts. To develop a model of AF associated with LV hypertrophy, we first induced pressure overload in mice by producing transverse aorta constriction (TAC) (25). On day 10, TAC-operated mice showed a significant increase in heart-to-body weight and LV wall thickness with preserved fractional shortening (Table 1). The atrium-to-body weight ratios were increased 36%, from 0.22 ± 0.02 mg/g in sham-operated mice (*n* = 5) to 0.30 ± 0.02 mg/g in TAC-operated mice (*n* = 5; *P* < 0.01), indicating that TAC operation induced hemodynamic overload in both the atrium and ventricle. We recorded ECGs using telemetry at 10 days after the operation, but no episode of spontaneous AF was observed in TAC- or sham-operated mice (Supplemental Figure 1; supplemental material available online with this article; doi:10.1172/JCI39942DS1).

To test the inducibility of AF, we applied programmed electrical stimulation directly to right atrium under Langendorff perfusion at 10 days after the operation. During the period for stabilization prior to stimulation, spontaneous episodes of AF were not observed in TAC- or sham-operated hearts. However, the induction of AF was attainable and reliably reproducible with programmed electrical stimulation of right atrium (Figure 1A). AF was defined as an episode of rapid and chaotic atrial rhythm and irregular ventricular response. AF was induced more frequently in TAC-operated hearts (100%) than in sham-operated hearts (20%) (Figure 1, A-C). In addition, the duration of AF episodes in TAC-operated hearts was significantly longer than that in sham-operated hearts (Figure 1D). We also applied atrial stimulation under Langendorff perfusion at 28 days after TAC operation. However, TAC-operated hearts showed severe LV dysfunction (fractional shortening, $16.6\% \pm 8.4\%$) at this time point, and undesirable arrhythmias such as ventricular fibrillation were induced each time after stimulation, which hampered our evaluation of AF arrhythmogenesis. Therefore, atrial burst stimulation under Langendorff perfusion at 10 days after TAC operation represents a valid *ex vivo* model that permits study of AF substrate, especially in the setting of LV hypertrophy.

Mast cells are accumulated and activated in the atrium of TAC-operated mice. To assess the contribution of mast cells to atrial arrhythmogenicity, we evaluated the contents of mast cells in atrium by staining histological sections with toluidine blue. The number of infiltrating mast cells showed a 2.5-fold increase in

TAC-operated mice on day 10, as compared with sham-operated mice (Figure 2A). Avidin conjugated to fluorochrome dyes binds to the negatively charged heparin proteoglycans and identifies the granules of mast cells (20, 26). In the left and right atria of TAC-operated mice, we observed a marked increase of mast cell activation with the presence of extruded avidin-positive granules close to cell surface (Figure 2B). These results suggest that mast cells are accumulated and activated in the atrium of pressure-overloaded hearts.

Stabilization of mast cells by cromolyn attenuates AF in TAC-operated hearts. Accumulation of mast cells in the atrium indicated a causal link between infiltration of these cells and the pathogenesis of AF. To determine the importance of mast cells in this process, we systemically administered the mast cell stabilizer cromolyn (14, 20) to TAC-operated

mice. In the atrium at 10 days after TAC operation, the degranulation of mast cells was almost completely inhibited by cromolyn treatment (Figure 2B), although the mast cell contents were not significantly decreased (*P* = 0.17; Figure 2A). Echocardiographic parameters regarding LV hypertrophy and systolic function remained unchanged by cromolyn treatment (Table 1). As revealed by histology, there was no significant difference in the average size of ventricular myocytes between cromolyn- and vehicle-treated mice (Supplemental Figure 2). In addition, the atrium-to-body weight ratios at 10 days after TAC operation were not significantly different between cromolyn- and vehicle-treated mice (0.30 ± 0.02 mg/g vs. 0.28 ± 0.02 mg/g; *P* = 0.43). These results suggest that cromolyn did not affect the hemodynamic workload. However, as compared with vehicle-treated mice, cromolyn-treated mice showed a remarkable reduction in the incidence and duration of AF episodes after atrial burst stimulation under Langendorff perfusion (Figure 3, A-C). To validate and extend our *ex vivo* findings, we subjected anesthetized mice to rapid transesophageal atrial pacing and simultaneous surface ECG recording at 10 days after the operation. AF could be induced *in vivo* after atrial burst stimulation in TAC-operated mice, but not in sham-operated mice (Figure 3, D-F). Similarly, cromolyn treatment completely suppressed AF induced by transesophageal atrial pacing in TAC-operated mice (Figure 3, G and H).

Atrial fibrosis is a major feature of structural remodeling that contributes to AF substrate (3, 4). In the atrium of TAC-operated mice, Masson's trichrome staining revealed areas of interstitial fibrosis (Figure 3I), and hydroxyproline assay indicated deposition of collagen (Figure 3J). Mast cell stabilization by cromolyn remarkably attenuated fibrotic changes in the atrium of TAC-operated mice (Figure 3, I and J). These results suggest that stabilization of mast cells prevents atrial structural remodeling and AF inducibility in TAC-operated mice.

Reconstitution with BM cells from mast cell-deficient W/W^v mice attenuates AF in TAC-operated hearts. To further examine the role of mast cells in AF, we utilized mast cell-deficient *WBB6F1-Kit^{fl}/W^v* (*W/W^v*) mice carrying compound heterozygous mutations of *c-kit* (*Kit^W*, null; *Kit^{fl}*, dominant negative). To circumvent the undesirable effects by altered *c-kit* signaling in nonhematopoietic cells, we reconstituted CS7BL/6 mice with BM cells from *W/W^v* mice or control *WBB6F1-Kit^{+/+}* (+/+) mice. We first confirmed, by tolu-

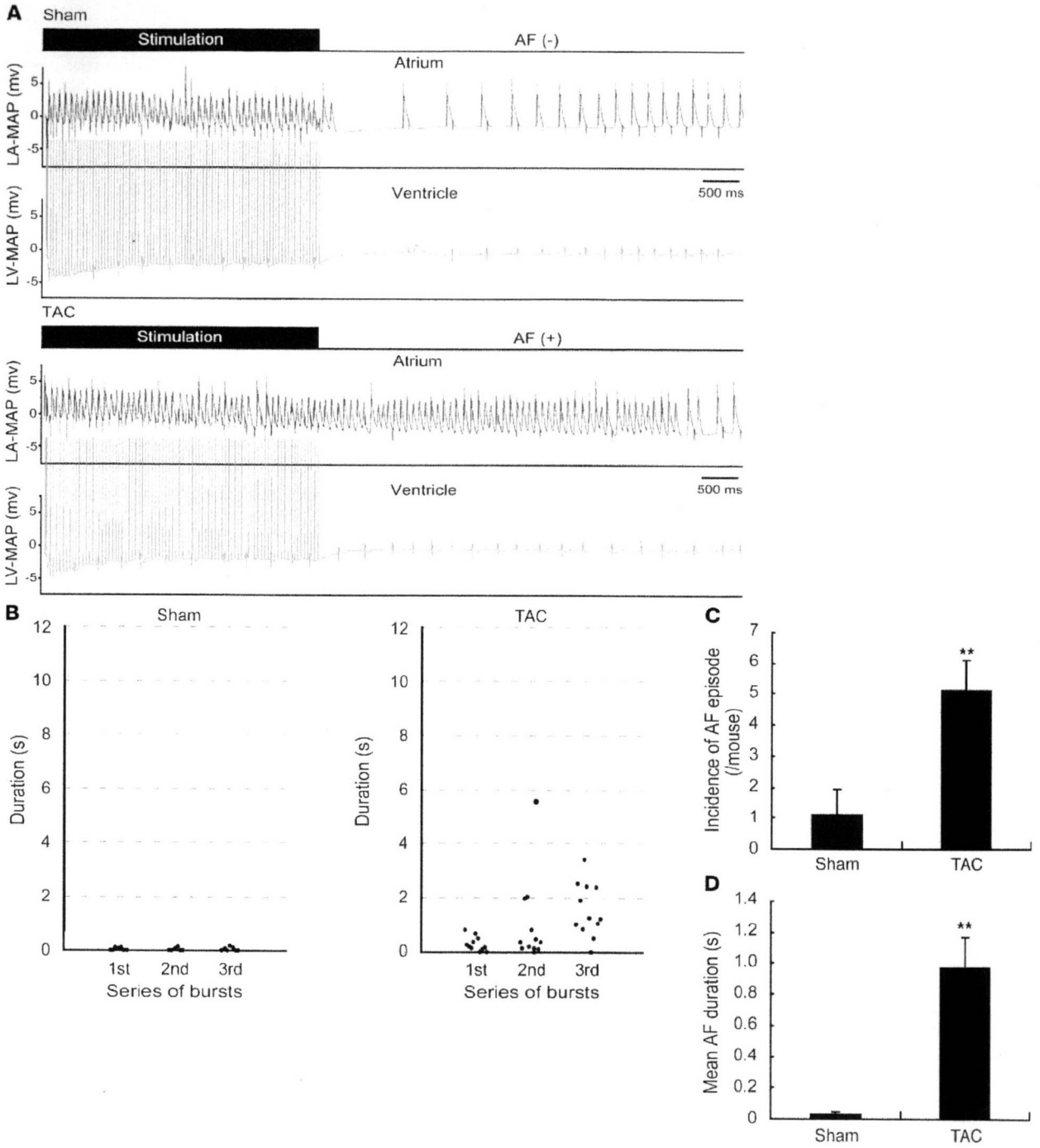


Figure 1
 Induction of AF in Langendorff-perfused hearts of mice after TAC operation. **(A)** Termination of the burst of atrial stimulation triggers AF, characterized by rapid and chaotic atrial rhythm and irregular ventricular response, in Langendorff-perfused hearts undergoing TAC operation (lower panels), but not sham operation (upper panels). LA-MAP, monophasic action potential of left atrium; LV-MAP, monophasic action potential of LV. **(B)** AF was triggered in mice undergoing TAC ($n = 5$) or sham ($n = 5$) operation by applying 3 series of bursts with 5-minute intervals. The duration of AF episode occurring after each burst is plotted. **(C)** Incidence of AF episodes during 3 series of bursts in mice undergoing TAC ($n = 5$) or sham ($n = 5$) operation. **(D)** Mean duration of AF episodes during 3 series of bursts in mice undergoing TAC ($n = 5$) or sham ($n = 5$) operation. ****** $P < 0.01$ versus sham. Data are presented as mean \pm SEM.

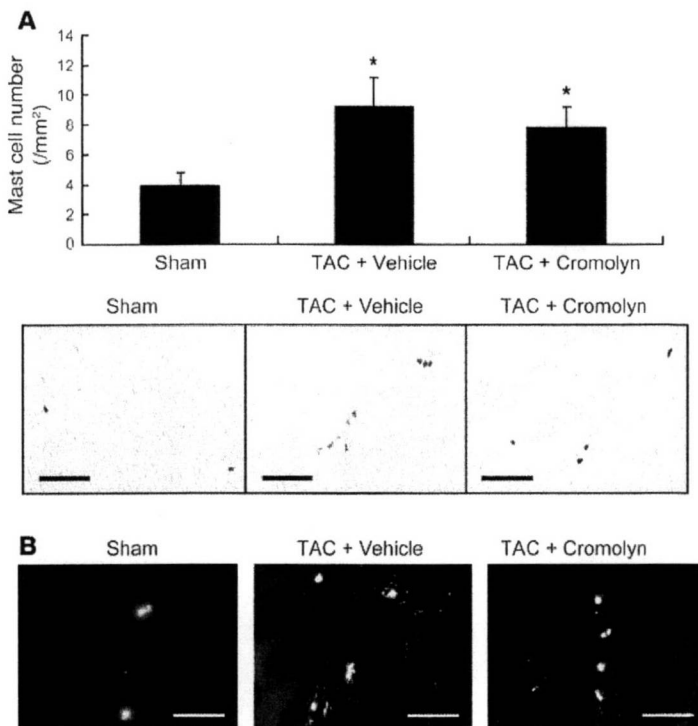


Figure 2

Stabilization of mast cells infiltrating the atrium of TAC-operated mice by cromolyn. **(A)** Representative histological sections with toluidine blue staining for detection of mast cells (purple) in the atrium. Wild-type mice were treated with cromolyn ($n = 7$) or vehicle ($n = 8$), and subjected to TAC operation. Mast cell content on day 10 was presented as mean \pm SEM. Sham-operated mice were used as control ($n = 5$). * $P < 0.05$ versus sham. **(B)** Rhodamine-avidin staining for visualization of mast cell degranulation. Scale bars: 10 μm (A); 5 μm (B).

idine blue staining, that mast cells were not present in the atrium of mice reconstituted with BM cells from W/W^v mice (W/W^v-BMT mice) after TAC operation, although abundant mast cells infiltrated the atrium of mice reconstituted with BM cells from +/+ mice (+/+BMT mice) after TAC operation (Figure 4A). Echocardiographic examination revealed that LV hypertrophy after TAC operation did not significantly differ between W/W^v-BMT and +/+BMT mice, but the fractional shortening in W/W^v-BMT mice was slightly decreased compared with that in +/+BMT mice (Table 2). In spite of the reduced LV systolic function after TAC operation, the atrium-to-body weight ratios were not significantly different between +/+BMT mice and W/W^v-BMT mice (0.27 ± 0.02 mg/g vs. 0.31 ± 0.05 mg/g; $P = 0.54$), and reconstitution with W/W^v BM induced a marked reduction in the incidence and duration of AF episode after atrial burst stimulation compared with +/+ BM reconstitution (Figure 4, B-D). In addition, histological analysis and hydroxyproline assay revealed that atrial fibrosis after TAC operation was attenuated in W/W^v-BMT mice compared with +/+BMT mice (Figure 4, E and F). These results suggest that deficiency of mast cells prevents atrial structural remodeling and AF inducibility in TAC-operated mice.

BM-derived mast cells cocultured with cardiac myocytes or fibroblasts release PDGF-A to promote fibrinogenesis. In response to a variety of stimuli, mast cells are activated and release numerous bioactive effectors that, either prestored or de novo synthesized, mediate

immunoregulatory and proinflammatory effects (11, 24). To delineate mast cell-derived effectors that are involved in the promotion of atrial fibrosis, we examined the gene expressions of fibrosis-related effectors in BM-derived mast cells (BMMCs) after coculture with cardiac myocytes or fibroblasts (Figure 5, A and B, and Supplemental Figure 3). Notably, in quantitative real-time RT-PCR analysis, the mRNA levels of murine *Pdgfa* in BMMCs were prominently elevated after 6 hours coculture with neonatal rat cardiac myocytes or fibroblasts (Figure 5, A and B, and Supplemental Figure 3). In addition, the expression levels of *Pdgfa* were upregulated in the atrium at 10 days after TAC operation, and they were significantly attenuated by reconstitution with W/W^v BM (Figure 5C). These results suggest that mast cells infiltrating the atrium are activated to increase *Pdgfa* gene expression.

Next, we assayed the concentrations of PDGF-AA in medium conditioned by coculture of BMMCs and cardiac fibroblasts. The PDGF-AA concentration showed a more than 3-fold increase after 6 hours coculture, and this increase was remarkably blunted by stabilization of BMMCs with cromolyn during the coculture (Figure 6A). The conditioned medium of coculture promoted cell proliferation of cardiac fibroblasts, and the proliferative effects were abrogated by addition of a neutralizing anti-PDGF α -receptor (anti-PDGFR- α) antibody to the conditioned medium (Figure 6B). Furthermore, the expression of *Col3a1* in cardiac fibroblasts was upregulated after coculture with BMMC, and it was blunted by the treatment with cromolyn or anti-PDGFR- α antibody (Figure 6C). Thus, BMMC-derived PDGF-A can induce cell proliferation and collagen gene expression in cardiac fibroblasts. These results raise a possibility that infiltrating mast cells promote atrial fibrosis and AF inducibility in a PDGF-A-mediated pathway.

Administration of PDGF-AA enhances AF susceptibility in normal hearts. To examine functional significance of atrial *Pdgfa* upregulation in the development of AF substrate, we administered PDGF-AA or vehicle to nonoperated mice and applied atrial burst stimulation. Administration of PDGF-AA for 10 days induced systemic tissue fibrosis, which was particularly prominent in atrium as compared with ventricle (Figure 7A). As a consequence, PDGF-AA-treated hearts showed a significant increase in the incidence and duration of AF episode after atrial burst stimulation under Langendorff perfusion compared with vehicle-treated hearts (Figure 7, B-D). These results suggest that upregulation of *Pdgfa* in atrium can induce atrial fibrosis and enhance AF inducibility in normal hearts.

Neutralization of PDGFR- α attenuates AF in TAC-operated hearts. Next, to examine the role of PDGF-A in the pathogenesis of AF substrate, we inhibited the actions of PDGF-A in TAC-operated hearts by systemic injection of a neutralizing antibody against PDGFR- α (APAS) (27). At 10 days after TAC operation, LV hypertrophy and contraction, as assessed by echocardiography, did not significantly differ between neutralizing antibody-treated mice (TAC-APAS mice) and control IgG2a-treated mice (TAC-IgG mice) (Table 3). In addition, the atrium-to-body weight ratios were not significantly different between TAC-APAS and TAC-IgG mice (0.34 ± 0.02 mg/g vs. 0.31 ± 0.03 mg/g; $P = 0.44$). However, neutralization of PDGFR- α induced a marked reduction

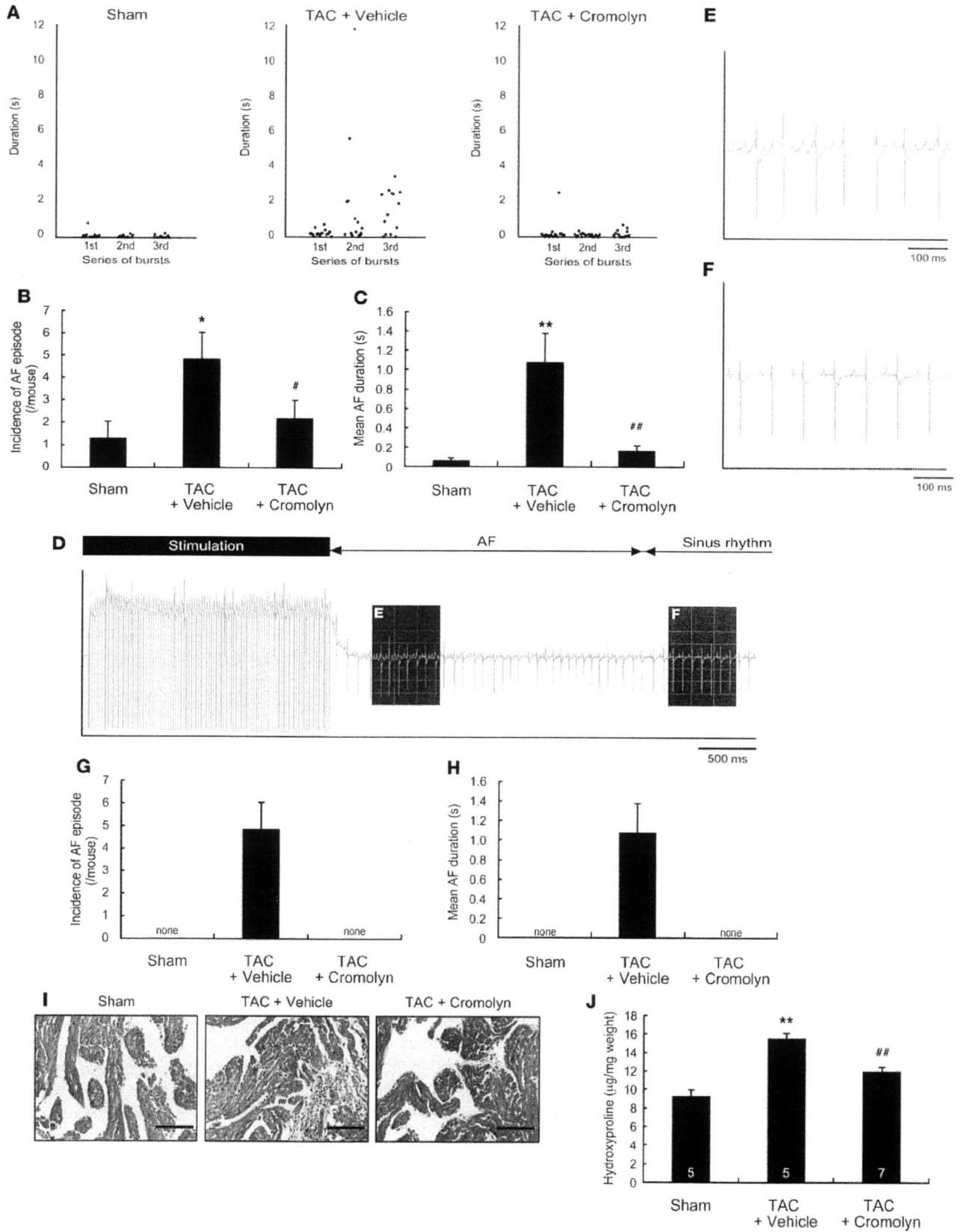




Figure 3

Attenuation of AF and atrial fibrosis by mast cell stabilization by cromolyn. **(A)** Scatter plot of the duration of AF episodes occurring during 3 series of bursts in Langendorff-perfused hearts ($n = 10$). **(B)** Incidence of AF episodes during 3 series of bursts under Langendorff perfusion ($n = 10$). * $P < 0.05$ versus sham; # $P < 0.05$ versus TAC treated with vehicle. **(C)** Mean duration of AF episodes during 3 series of bursts under Langendorff perfusion ($n = 10$). ** $P < 0.01$ versus sham; ## $P < 0.01$ versus TAC treated with vehicle. **(D)** Representative surface ECG in lead-II deflection of AF induced by termination of the burst of transesophageal atrial pacing in TAC-operated mice. **(E)** High-magnification view of the section delineated by shaded box in **D**, showing AF with chaotic atrial rhythm and irregular ventricular response. **(F)** High-magnification view of the section delineated by shaded box in **D**. AF was spontaneously converted to sinus rhythm. **(G)** Incidence of AF episodes during 3 series of transesophageal bursts ($n = 6$). **(H)** Mean duration of AF episodes during 3 series of transesophageal bursts ($n = 6$). **(I)** Representative histological sections with Masson's trichrome staining for visualization of atrial fibrosis (blue staining). Scale bars: 20 μm . **(J)** Hydroxyproline content in the atrium. Number of mice for each experiment is indicated in the bars. ** $P < 0.01$ versus sham; ## $P < 0.01$ versus TAC treated with vehicle. Data are presented as mean \pm SEM.

in the incidence and duration of AF episode both after atrial burst stimulation under Langendorff perfusion (Figure 8, A–C) and after transesophageal atrial pacing in vivo (Figure 8, D and E). In addition, histological analysis and hydroxyproline assay revealed that atrial fibrosis was attenuated in TAC-APA5 mice compared with TAC-IgG mice (Figure 8, F and G). Thus, the effects of cromolyn treatment or BM reconstitution from W/W^v mice on AF substrate were reproduced by neutralization of PDGFR- α in TAC-operated hearts. These results suggest that PDGF-A mediates the deleterious effects of mast cells to promote atrial fibrosis and AF inducibility.

Discussion

Clinical and experimental studies have suggested that inflammation underlies a susceptible AF substrate, which is characterized by interstitial fibrosis in atrium. Our present study demonstrated a hitherto unknown role of mast cells in the development of a susceptible AF substrate. Mast cells were accumulated and activated in the atrium of pressure-overloaded mice, and pharmacological stabilization or genetic depletion of mast cells prevented atrial structural remodeling and reduced the incidence and duration of AF following atrial burst stimulation. Notably, infiltrating mast cells induced upregulation of PDGF-A in the atrium, and neutral-

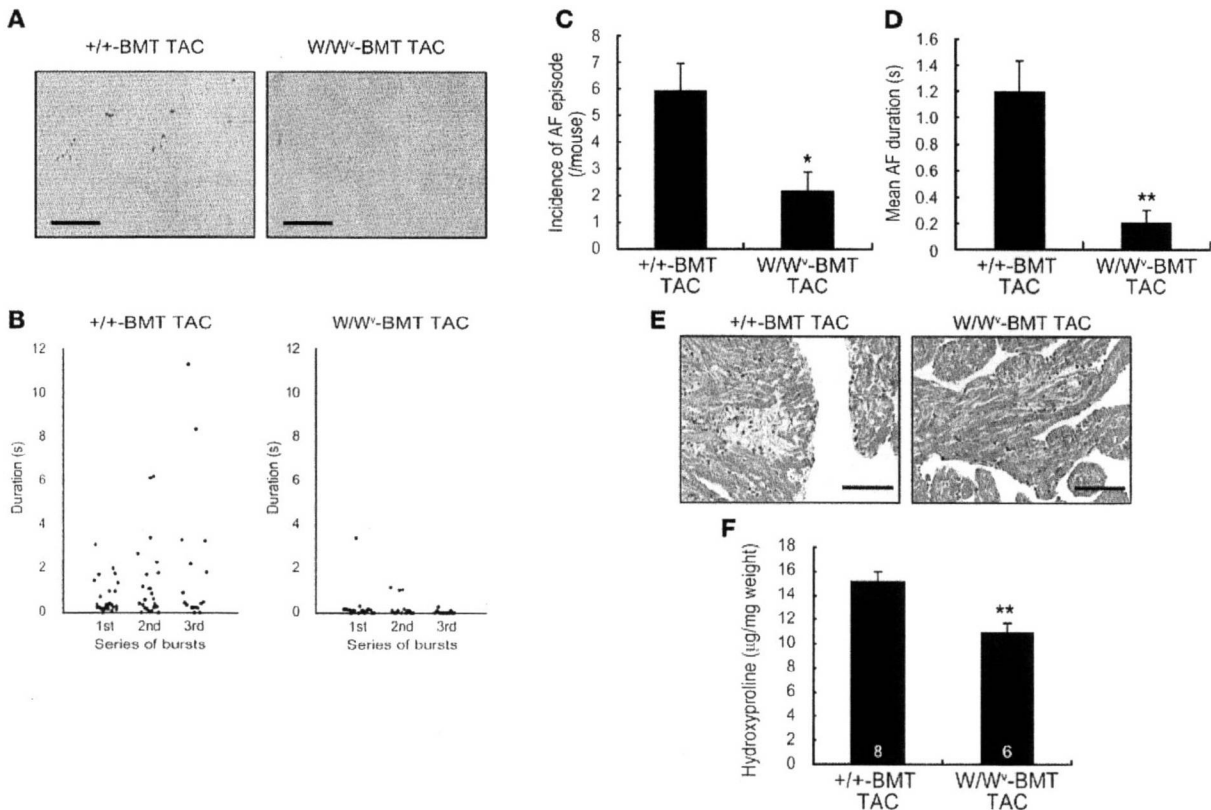


Figure 4

Attenuation of atrial fibrosis and AF by reconstitution with BM cells from W/W^v mice. **(A)** Representative histological sections with toluidine blue staining. Mast cells were not present in the atrium of TAC-operated W/W^v-BMT mice. **(B)** Scatter plot of the duration of AF episodes occurring during 3 series of bursts in TAC-operated W/W^v-BMT mice ($n = 11$) or +/+BMT mice ($n = 11$). **(C)** Incidence of AF episodes during 3 series of bursts ($n = 11$). * $P < 0.05$ versus +/+BMT mice. **(D)** Mean duration of AF episodes during 3 series of bursts ($n = 11$). ** $P < 0.01$ versus +/+BMT mice. **(E)** Representative histological sections with Masson's trichrome staining for visualization of atrial fibrosis (blue staining). **(F)** Hydroxyproline content in the atrium. Number of mice for each experiment is indicated in the bars. Scale bars: 10 μm (**A**); 20 μm (**E**). Data are presented as mean \pm SEM.



Table 2
Echocardiographic measurements in TAC- or sham-operated W/W^v-BMT or +/-BMT mice

	Sham		TAC	
	+/-BMT	W/W ^v -BMT	+/-BMT	W/W ^v -BMT
Number	9	9	9	9
HW/BW (mg/g)	4.42 ± 0.14	4.42 ± 0.13	5.51 ± 0.10 ^A	5.34 ± 0.16 ^A
HR (bpm)	636.63 ± 7.78	629.22 ± 2.89	613.20 ± 9.34	612.33 ± 6.78
LVDd (mm)	3.68 ± 0.05	3.61 ± 0.07	3.55 ± 0.07	3.69 ± 0.07
LVDs (mm)	2.30 ± 0.05	2.15 ± 0.05	2.05 ± 0.04 ^A	2.28 ± 0.08 ^B
FS (%)	39.3 ± 0.93	40.4 ± 0.44	41.6 ± 0.26 ^C	38.96 ± 1.32 ^D
LVPWth (mm)	0.61 ± 0.01	0.58 ± 0.01	0.68 ± 0.01 ^A	0.66 ± 0.02 ^A

^AP < 0.01 versus sham. ^BP < 0.01 versus TAC-operated +/-BMT. ^CP < 0.05 versus sham. ^DP < 0.05 versus TAC-operated +-BMT.

ization of PDGFR- α prevented atrial fibrosis and AF inducibility, indicating a pivotal role of PDGF-A in mast cell-triggered AF. It has been reported that atrial arrhythmias and fibrillation occur with extremely low frequency in mice because the atrium is too small in size to maintain multiple-circuit reentry (28). Indeed, we did not detect any spontaneous episode of AF in TAC-operated mice by ECG telemetry (Supplemental Figure 1), but atrial burst

stimulation reproducibly induced AF either in ex vivo or in vivo hearts subjected to pressure overload (Figures 1 and 3). Although the duration of AF was limited in length as compared with that in large animal models, a mouse model is powerful for dissection of the causal relationship between arrhythmogenesis and genetic or cellular factors. Although transesophageal pacing in vivo is minimally invasive for atrial stimulation, the incidence of AF was relatively low even in TAC-operated mice (50%), and an anesthetic agent might influence the inducibility and duration of AF in an in vivo model (28). In this regard, atrial stimulation under Langendorff perfusion is a suitable and reliable model of AF that provides mechanistic and therapeutic insights into development of an AF substrate in the setting of hemodynamic overload.

Besides orchestrating allergic and immune responses, mast cells participate in the inflammatory process that underlies the development of cardiovascular diseases (11). Inasmuch as the number of infiltrating mast cells at the affected lesions is significantly increased but yet relatively low, it has been difficult to characterize the relevance of these cells to the pathogenesis of a disease. However, mice genetically deficient for mast cells allow assessment of

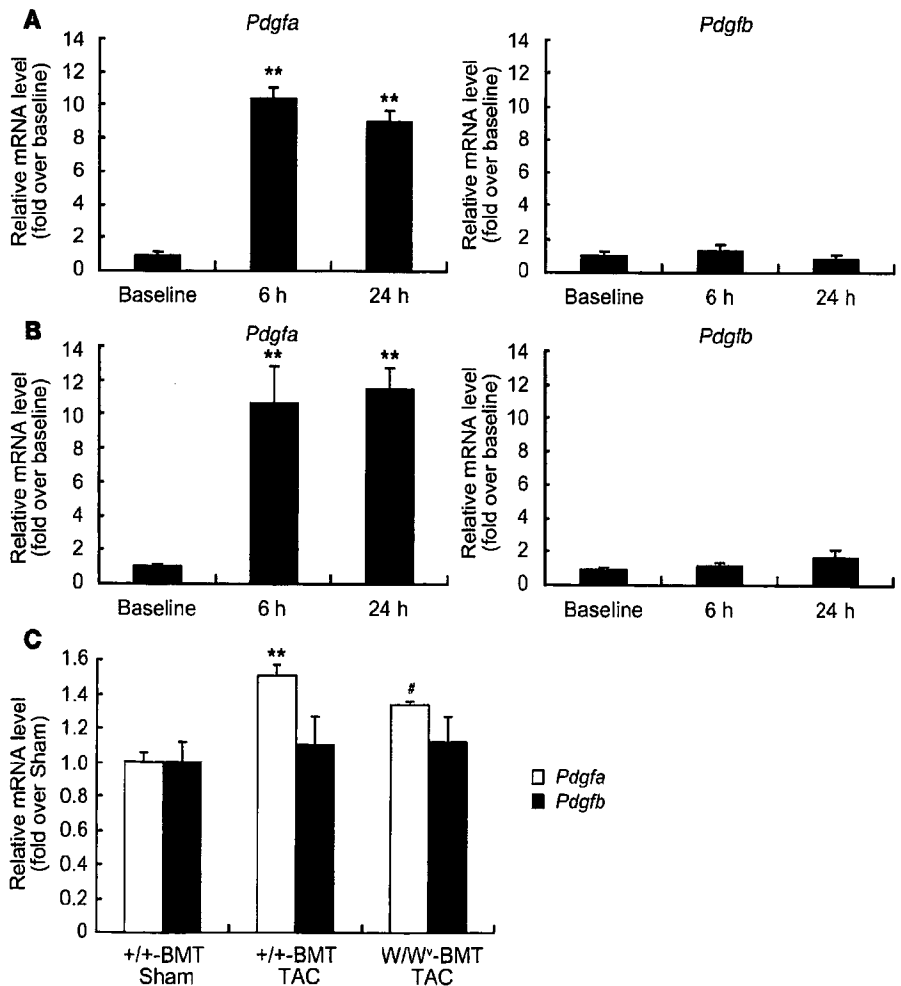
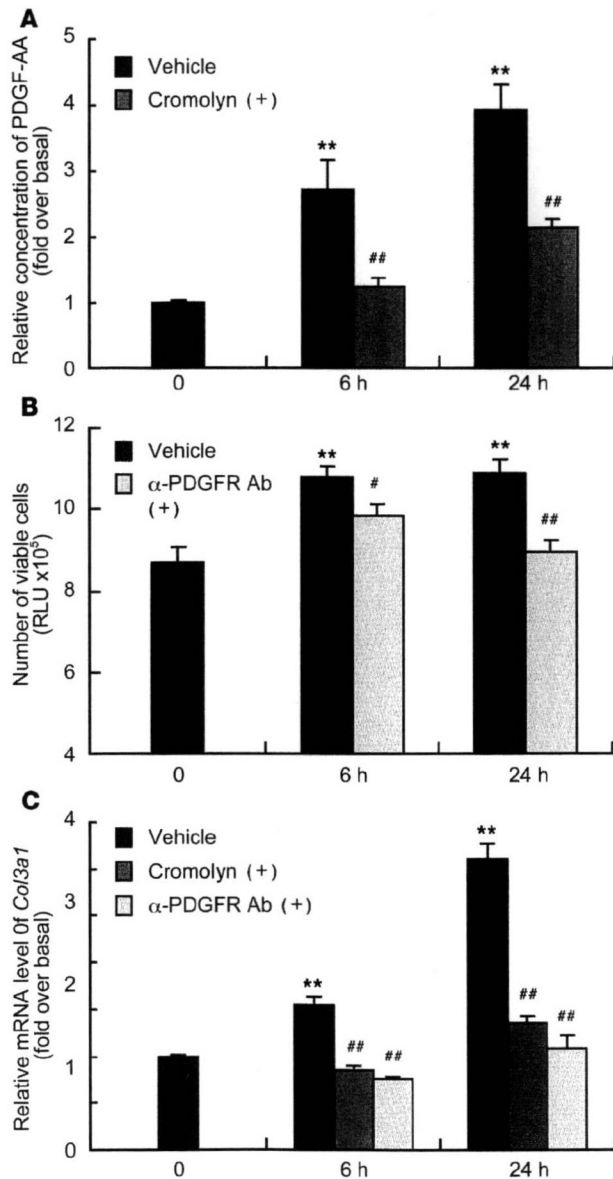


Figure 5
Mast cell-mediated upregulation of *Pdgfa* expression in the atrium of TAC-operated hearts. (A) mRNA expression of *Pdgfa* and *Pdgfb* in BMMCs at baseline, 6 hours, and 24 hours after coculture with cardiac myocytes. Experiments were repeated 4 times in triplicate. **P < 0.01 versus baseline. (B) mRNA expressions of *Pdgfa* and *Pdgfb* in BMMCs at baseline, 6 hours, and 24 hours after coculture with cardiac fibroblasts. Experiments were repeated 5 times in triplicate. **P < 0.01 versus baseline. (C) mRNA expressions of *Pdgfa* and *Pdgfb* in the atrium of sham-operated mice (n = 8), TAC-operated W/W^v-BMT mice (W/W^v-BMT TAC, n = 7), or +/- mice (+/-BMT TAC, n = 6). **P < 0.01 versus sham; #P < 0.05 versus +/-BMT TAC. Data are presented as mean ± SEM.

**Figure 6**

BMMC-derived PDGF-A can induce cell proliferation and collagen gene expression in cardiac fibroblasts. **(A)** ELISA analysis of PDGF-AA content in conditioned medium at baseline, 6 hours, and 24 hours after coculture of BMDCs and cardiac fibroblasts with or without cromolyn (10 μ M). Experiments were repeated 5 times in triplicate. ** P < 0.01 versus baseline; ## P < 0.01 versus vehicle. **(B)** Number of viable cardiac fibroblasts at baseline, 6 hours, and 24 hours after culture in medium-conditioned coculture of BMDCs and cardiac fibroblasts with or without a neutralizing anti-PDGFR- α antibody (2 μ g/ml), as assessed by relative amount of ATP. Experiments were repeated 4 times in triplicate. ** P < 0.01 versus baseline; # P < 0.05; ## P < 0.01 versus vehicle. **(C)** mRNA expressions of *Col3a1* in cardiac fibroblasts cocultured with BMDCs with or without cromolyn (10 μ M) or a neutralizing anti-PDGFR- α antibody (2 μ g/ml) at baseline, 6 hours, and 24 hours. Experiments were repeated 4 times in triplicate. ** P < 0.01 versus baseline; ## P < 0.01 versus vehicle. Data are presented as mean \pm SEM.

Mast cells are long lived in the tissue and can reenter cell cycle and proliferate locally (34). A variety of chemokines have been identified that induce local recruitment of mast cells, such as SCF, monocyte chemoattraction protein-1 (MCP-1), nerve growth factor (NGF), and RANTES (24). In addition, interactions between mast cells and connective tissue matrix components have profound influences on the distribution of mast cells in tissues (35–37). Although the most important trigger for mast cell activation is antigen- and IgE-dependent aggregation of IgE receptor (Fc ϵ RI), mast cells can be activated by various factors, such as cytokines, growth factors, and hormones (11, 12, 24). In our study, coculture with cardiac myocytes or fibroblasts per se promoted gene expression of some cytokines in BMDCs. We postulate that a certain paracrine- or cell-to-cell contact-dependent signaling may trigger mast cell activation in hearts. Further investigation will be required to delineate the precise mechanisms of how cardiac mast cells are accumulated and activated in stressed hearts.

Mast cells secrete diverse chemical mediators, cytokines, and growth factors upon exposure to a stimulus. This process involves release of the mediators prestored in the granules (degranulation) and de novo synthesis of mediators. Differential synthesis of mast cell mediators is dependent on the particular mechanism of activation and the strength of the stimulus and is crucially involved in the inflammatory process (12, 24). We identified PDGF-A as a crucial molecule that mediates mast cell-induced atrial fibrosis. Among the fibrogenic mediators, upregulation of *Pdgfa* in BMDCs was pronounced after coculture either with cardiac myocytes or fibroblasts. In our coculture experiments, BMMC-derived PDGF-A accelerated proliferation of cardiac fibroblasts and stimulated synthesis of type III collagen in cardiac fibroblasts. PDGF-A dimeric isoform (PDGF-AA) selectively binds to PDGFR- α (38), and PDGF-AA infusion exerted potent fibrogenic effects, particularly on atrium (Figure 7A), consistent with a previous paper demonstrating that atrial fibroblasts showed higher reactivity to PDGF than ventricular fibroblasts (39). Importantly, the mRNA levels of *Pdgfa* in atrium were significantly increased after TAC operation, which was blunted by depletion of mast cells by BM reconstitution from W/W^v mice. PDGF-A production in atrium is critically relevant to the AF pathogenesis of pressure-overloaded hearts because neutralization of PDGFR- α prevented atrial fibrosis and AF. Collectively, our results suggest that atrial mast cells induce upregulation

the contributions of mast cell function to biological responses in vivo (11). In this study, we utilized *c-kit* mutant W/W^v mice that are profoundly mast cell deficient (29) and virtually lack melanocytes and interstitial Cajal cells (30). According to a recent paper, *c-kit* is also expressed in cardiac stem cells and cardiac myocytes and plays a regulatory role in the differentiation of these cells (31). Thus, to avoid the effects of *c-kit* mutation on cardiac myocytes, we reconstituted C57BL/6 mice with BM from W/W^v mice. BM reconstitution from W/W^v mice influenced contractile function, which might be related to hematological abnormalities such as macrocytic anemia (32). In spite of the hemodynamic burden, atrial structural remodeling and AF susceptibility were blunted by BM reconstitution from W/W^v mice, which underpinned the functional importance of mast cells in the AF pathogenesis of pressure-overloaded hearts.

Mast cells exist in the heart under physiological conditions (13), and mast cell density in heart tissues of patients with cardiomyopathy is elevated, as compared with normal hearts (33).

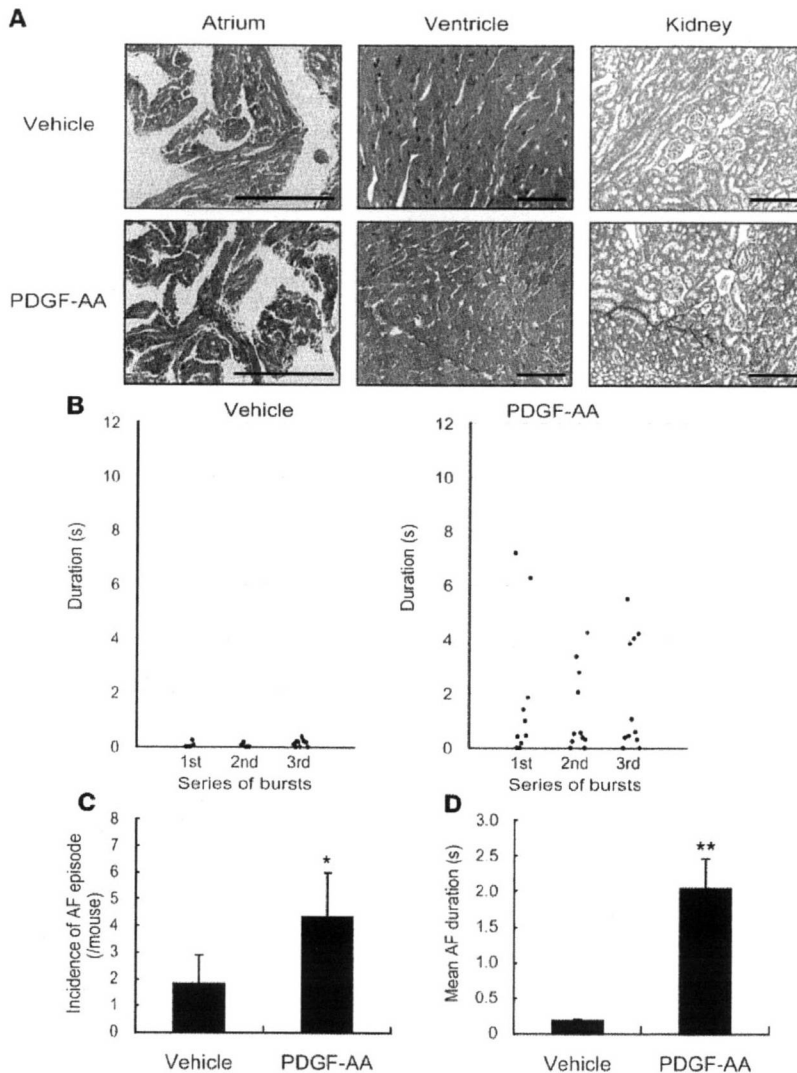


Figure 7

Systemic administration of PDGF-AA induces atrial fibrosis and enhances AF susceptibility in Langendorff-perfused hearts. **(A)** Representative histological sections with Masson's trichrome staining for visualization of fibrosis (blue staining) in the atrium, ventricle, and kidney of mice administered PDGF-AA or vehicle. Scale bars: 20 μ m. **(B)** Scatter plot of the duration of AF episodes occurring during 3 series of bursts in mice administered PDGF-AA ($n = 6$) or vehicle ($n = 6$). Duration of AF episodes occurring after each burst are plotted. **(C)** Incidence of AF episodes during 3 series of bursts in mice administered PDGF-AA ($n = 6$) or vehicle ($n = 6$). **(D)** Mean duration of AF episodes during 3 series of bursts in mice administered PDGF-AA ($n = 6$) or vehicle ($n = 6$). Data are presented as mean \pm SEM. * $P < 0.05$ versus vehicle; ** $P < 0.01$ versus vehicle.

of *Pdgfa*, leading to progression of a susceptible AF substrate in pressure-overloaded hearts. At present, it remains uncertain whether atrial mast cells are the sole source of PDGF-A. Indeed, mast cell activation can influence the function of many different cell types (12, 24), and especially, macrophages may serve as a source of PDGF-A (38). Further studies using an intricate genetic model to delete *Pdgfa* specifically in mast cells will be required to dissect the importance of mast cell-derived PDGF-A in the pathogenesis of AF.

Several clinical studies have proved the efficacy of pharmacological inhibition of the renin-angiotensin system in the prevention of atrial fibrosis and promotion of AF (40). The therapeutic approach to attenuating or reversing the AF substrate is appealing. Our study highlighted the pathogenic role of mast cells in promoting the AF substrate in pressure-overloaded hearts. Of course, this observation must be further investigated in future studies using large animal models for testing applicability to clinical conditions because variability among species and experimental models may give rise to differences in anatomical and electrophysiological parameters (41). As a starting point for

investigations, we propose that the mast cell-PDGF-A axis will be a promising therapeutic target for the upstream prevention of AF in stressed hearts.

Methods

Mice, TAC operation, and echocardiography. All of the experimental protocols were approved by the Institutional Animal Care and Use Committee of Chiba University. CS7BL/6 mice, mast cell-deficient W/W^v mice, and congenic $+/+$ littermates were purchased from Japan SLC. For TAC operation, 10-week-old male mice were anesthetized by i.p. injection of pentobarbital, and respiration was artificially controlled with a tidal volume of 0.2 ml and a respiratory rate of 110 breaths/min. The transverse aorta was constricted with 7-0 nylon strings by ligating the aorta with splinting a blunted 27-gauge needle, which was removed after the ligation. After aortic constriction, the chest was closed and mice were allowed to recover from anesthesia. We confirmed that the magnitude of initial pressure elevation after aortic banding was identical in all groups of mice. The surgeon had no information about the mice used in this study. For evaluation of cardiac dimensions and contractility, transthoracic echocardiography was performed on conscious mice with the Vevo 770 Imaging System using a 25-MHz linear probe (Visual Sonics).